Advanced Analysis and Control Methods of AC Microgrids for Power Sharing Performance Improvement

Yuan, Wenbin

DOI (link to publication from Publisher):
10.54337/aau519581798

Publication date:
2022

Document Version
Publisher's PDF, also known as Version of record

ADVANCED ANALYSIS AND CONTROL METHODS OF AC MICROGRIDS FOR POWER SHARING PERFORMANCE IMPROVEMENT

BY
WENBIN YUAN

DISSERTATION SUBMITTED 2022

AALBORG UNIVERSITY
DENMARK

ADVANCED ANALYSIS AND CONTROL METHODS OF AC MICROGRIDS FOR POWER SHARING PERFORMANCE IMPROVEMENT

PH.D. THESIS

by

Wenbin Yuan

AALBORG UNIVERSITY
DENMARK

Dissertation submitted 2022

.

Dissertation submitted: December 2022

PhD supervisor: Professor Zhe Chen
Aalborg University

Assistant PhD supervisor: Assistant Professor Yanbo Wang
Aalborg University

PhD committee: Associate Professor Sanjay Kumar Chaudhary
Aalborg University, Denmark

Professor Seddik Bacha
University of Grenoble, France

Researcher Mauro Cappelli
Frascati Research Center, Italy

PhD Series: Faculty of Engineering and Science, Aalborg University

Department: AAU Energy

ISSN (online): 2446-1636
ISBN (online): 978-87-7573-785-7

Published by:
Aalborg University Press
Kroghstræde 3
DK – 9220 Aalborg Ø
Phone: +45 99407140
aauf@forlag.aau.dk
forlag.aau.dk

Printed in Denmark by Stibo Complete, 2022

CV

Wenbin Yuan was born in Henan Province, China. He graduated from Xiangtan University, Xiangtan, China, with the B.Eng. degree in 2015. Then he received M.Sc. degree from the School of Automation, Central South University, Changsha, China, in 2018. Currently, he is working toward Ph.D. degree in the Department of Energy, Aalborg University, Denmark. He focuses on research about distributed power generation systems, microgrids, as well as controller design of power electronic-based power systems.

ENGLISH SUMMARY

With the increasing exploitation of renewable energies, distributed power generation and power-electronics developments leads to innovative concepts of microgrids. The emerging microgrid concept can promote integration of renewable energies into the utility grid. However, there are also challenges to execute microgrids. At converter control level, accurate power sharing performance is important for converter lifetime but can be affected seriously by increasingly used nonlinear components. At system optimization level, power distribution ratio can be optimized for system efficiency and operation cost, which are highly coupled and cannot be optimized by independent optimization of either of them. Therefore, it is necessary to develop analysis and control methods for desired power control performance in microgrids both at converter level and system level.

The aim of this project is to develop advanced control methods to improve power sharing performance of microgrids considering nonlinear components impacts and efficiency and cost optimization. The thesis is organized as follows. Chapter 1 introduces the background, challenges and objectives of this project. The thesis outline is also presented in this chapter. Chapter 2 analyzes the influence of filter inductor nonlinearity on system power distribution performance. And a robust droop controller is designed to ensure accurate reactive power distribution performance regardless of impacts of nonlinear filter inductors. Chapter 3 establishes an efficiency model to analyze the core relationship between power distribution ratio and system efficiency. An efficiency-prioritized droop controller is further developed to reduce system power loss by adjusting power control references dynamically. Chapter 4 presents a self-optimization droop controller to enhance system performance considering efficiency and cost together according to proposed multi-objective optimization model. Chapter 5 summarizes conclusions of this research and explains potential future research topics.

The contributions of this project are drawn as follows. (1) The power distribution performance of microgrids is analyzed under impacts of nonlinear filter inductors. (2) The reactive power distribution deviation caused by nonlinear inductor is mitigated so that the system power control performance is ensured even with cost-effective nonlinear filter inductors. (3) The optimization conditions of maximum system efficiency are derived based on the core causation between power distribution performance and system efficiency. (4) System efficiency is improved by decentralized controller without using communication devices. (5) The coupling behaviour of system efficiency and operation cost is analyzed and the overall system performance is improved with consideration of efficiency and cost at the same time.

DANSK RESUME

Med den stigende udnyttelse af vedvarende energi, distribueret elproduktion og udvikling af el-elektronik fører til innovative koncepter for mikronetværk. Det nye koncept for mikronet kan fremme integrationen af vedvarende energikilder i forsyningsnettet. Der er imidlertid også udfordringer forbundet med gennemførelsen af mikronet. På konverterstyringsniveau er det vigtigt for konverterens levetid, at den nøjagtige effektfordeling er god, men den kan blive alvorligt påvirket af de stadig mere anvendte ikke-lineære komponenter. På systemoptimeringsniveau kan strømfordelingsforholdet optimeres med henblik på systemets effektivitet og driftsomkostninger, som er stærkt koblet og ikke kan optimeres ved uafhængig optimering af nogen af dem. Derfor er det nødvendigt at udvikle analyse- og kontrolmetoder til at opnå den ønskede effektstyringsydelse i mikronet både på konverterniveau og systemniveau.

Formålet med dette projekt er at udvikle avancerede styringsmetoder til at forbedre strømfordelingsydelsen i mikronet under hensyntagen til ikke-lineære komponenters indvirkning og optimering af effektivitet og omkostninger. Afhandlingen er organiseret som følger. I kapitel 1 introduceres baggrunden, udfordringerne og målene for dette projekt. I dette kapitel præsenteres også afhandlingens hovedlinjer. Kapitel 2 analyserer indflydelsen af filterinduktorens ikke-linearitet på systemets effektstyringsydelse. Og en robust droop-controller er designet til at sikre nøjagtig reaktiv effektfordeling uanset påvirkningerne fra ikke-lineære filterinduktorer. I kapitel 3 opstilles en effektivitetsmodel til analyse af det centrale forhold mellem effektfordelingsforholdet og systemets effektivitet. Der udvikles endvidere en effektivitetsprioriteret droop-regulator til at reducere systemets effekttab ved dynamisk at justere effektstyringsreferencerne. I kapitel 4 præsenteres en selvoptimerende droop-regulator til forbedring af systemets ydeevne under hensyntagen til effektivitet og omkostninger i overensstemmelse med den foreslåede optimeringsmodel med flere mål. Kapitel 5 opsummerer konklusionerne af denne forskning og forklarer potentielle fremtidige forskningsemner.

De vigtigste bidrag fra dette projekt er følgende. (1) Strømstyringsydelsen af mikronetværk analyseres under påvirkninger af ikke-lineære filterinduktorer. (2) Den reaktive effektfordelingsafvigelse forårsaget af ikke-lineære induktorer afbødes, så systemets effektstyringsydelse sikres selv med omkostningseffektive ikke-lineære filterinduktorer. (3) Optimeringsbetingelserne for maksimal systemeffektivitet er afledt på grundlag af kerneforholdet mellem effektfordelingsydelse og systemeffektivitet. (4) Systemeffektiviteten forbedres af decentral styring uden brug af kommunikationsenheder. (5) Koblingsadfærden for systemeffektivitet og

driftsomkostninger analyseres, og den samlede systemydelse forbedres under hensyntagen til effektivitet og omkostninger på samme tid.

ACKNOWLEDGEMENTS

This Ph.D. thesis is a summary of my research during the last three years, based on the Ph.D. project 'Advanced Analysis and Control Methods of AC Microgrids for Power Sharing Performance Improvement'.

Firstly, I would love to give my gratitude to my supervisors Professor Zhe Chen and Assistant Professor Yanbo Wang, who have given me professional and necessary help throughout the research. Their support is the key to completing the Ph.D. project. Their encouragement is the light for me to go through the dark night. It is my great honor to work with them. I would also like to thank Professor Claus Leth Bak. Together with my supervisors, he has supported me on many important decisions for my life and career.

I am also grateful to my colleagues Mr. Haoyuan Yu, Mr. Hanwen Zhang, Dr. Sinha Rakesh and Dr. Karthikeyan Nainar. They have offered me huge help on my research and daily life. It has been a joy to share an office with them.

Special thanks to my friends Dr. Zhongting Tang, Dr. Yi Zhang, Dr. Mengxing Chen, Dr. Yue Hu, Dr. Hanyu Zhou, Ms. Yunfeng Li, Mr. Qingyue Chen, Ms. Shuangshuang Xu, Ms. Ida Christiansen and Ms. Camilla Frandsen. They have made my life colorful and wonderful during the last three years.

Moreover, many thanks to all the colleagues at AAU Energy, for their kind help and support.

Finally, my gratitude goes to my parents and sisters for their support, encouragement and love.

Wenbin Yuan

July 23, 2020
Department of Energy, Aalborg University
Aalborg Øst, Denmark

TABLE OF CONTENTS

TABLE OF FIGURES

Fig. 4.4. Circuit configuration of the simulation test.

Fig. 4.5. Simulation results [74]. (a) Active-power distribution with traditional droop controller. (b) Reactive-power distribution with traditional droop controller. (c) Active-power distribution with proposed controller. (d) Reactive-power distribution with proposed controller. (e) Comprehensive performance factor with traditional and proposed controller. (f) System efficiency with traditional and proposed controller. (g) Operation cost with traditional and proposed controller.

Chapter 1. Introduction

1.1. BACKGROUND

With increasing concern about climate issues and green energy transformation, renewable energy is integrated into power systems with a significantly increasing penetration. Distributed power systems like microgrids are becoming an imperative solution to improve renewable energy penetration in a reliable and scalable way. Microgrids can be classified as DC microgrids, AC microgrids and hybrid AC/DC microgrids, which can work in islanded mode and grid-connect mode [1],[2]. AC microgrid is an important part of large-scale implementation of microgrid technologies since it can be built based on the techniques, standards and infrastructures of the existing power system. This thesis aims to solve key issues in AC microgrids. Fig. 1.1 shows the overview of an AC microgrid, consisting of dispatchable power generators, undispatchable power generators, energy storage system (ESS) and local loads. The hierarchical control structure is normally used in microgrids to achieve different control objectives and different time-scale control requirements [3]. The primary level consists of local controllers which are usually based on droop controllers to perform proportional power sharing and ensure that voltage and frequency operate within acceptable deviation range. The second level is usually responsible for voltage/frequency compensation and seamless transition between grid-integrated mode and islanded mode. The tertiary level monitors and manages power flow between different microgrids and the main grid. In this thesis, we focus on the primary level control method desigen of AC microgrid in islanded mode.

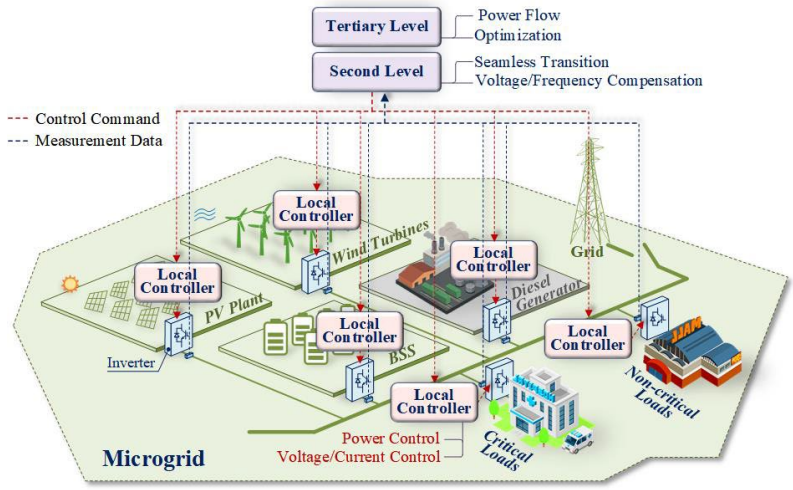

Fig. 1.1. Overview of an AC microgrid.

1.2. CHALLENGES AND MOTIVATIONS

Despite potential advantages of AC microgrids, there are some technical challenges that need to be addressed. Among these challenges, power control performance is a key concern of microgrids as it is important for system reliability, stability, efficiency and cost. There are two open questions when it comes to the power control performance of microgrids, as shown in Fig. 1.2. The first one is at converter level, which is how to perform desired power sharing performance despite different behaviours of paralleled converters. These different behaviours can be caused by different parameters of converters, mismatched cable parameters, different working conditions of DGs, etc. The second one is at system level, which is how to set power distribution references considering different optimization objectives such as reliability, stability, efficiency, cost, etc. The aims of this thesis are based on the two open questions, which are: (1) Study the power sharing behaviour of microgrids under nonlinear operation conditions. (2) Implement desired power sharing performance despite nonlinear filter inductors. (3) Investigate the relationship between power sharing behaviour and system efficiency and cost. (4) Improve system performance including efficiency and cost by local controller.

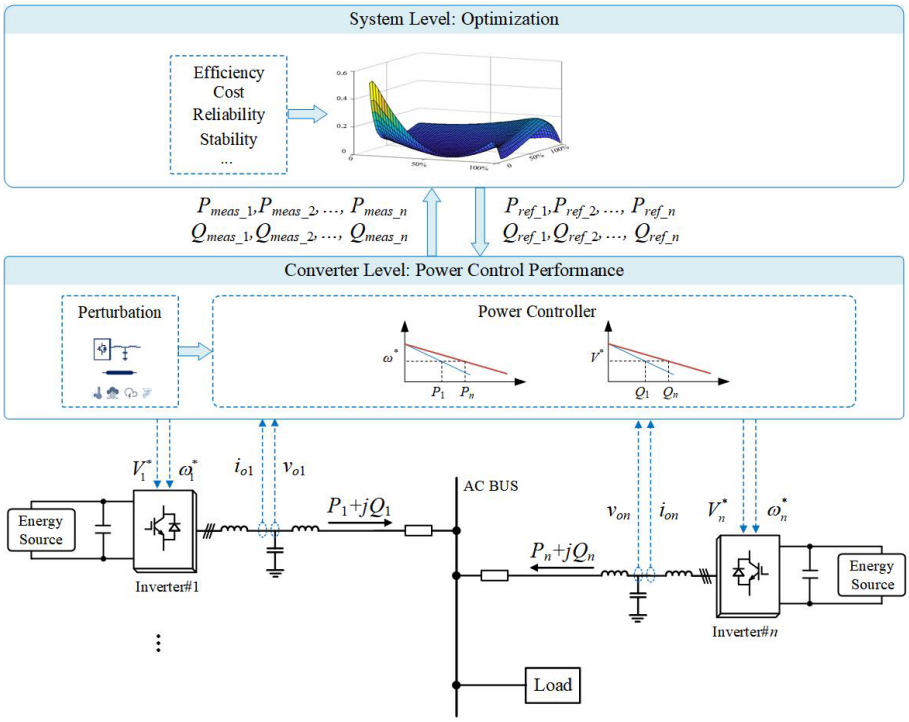

Fig. 1.2. Open questions in AC microgrids.

1.2.1. POWER CONTROL ISSUE OF MICROGRIDS

Power sharing performance is one of the most important concerns of microgrids because it is the key technique to implement well-behaviour microgrids including high reliability, high efficiency, low operation cost, etc. Various droop control methods are widely used because of advantages such as good active power sharing performance, easy implementation, communication free, etc. However, it is hard to perform desired reactive power sharing performance because it can be affected by mismatched feeder impedances [4]-[6], load profiles [7]-[8] or nonlinear components [9]-[10].

There have been various control strategies to deal with the reactive power sharing issue [4]-[14]. In [4]-[6], virtual impedance-based controllers are developed to ensure reactive power sharing performance by utilizing virtual impedance loop to reshape impedance characteristics of converters. In [7], an optimal controller is presented to perform accurate reactive power distribution for multi-bus system based on distributed communication. In [8], a signal injection method is presented to improve power sharing performance under both linear and nonlinear loads. In addition, controllers are developed in [11]-[14] for accurate reactive power allocation by dynamically optimizing virtual impedance through low bandwidth communication channels. However, existing works mainly focus on reactive power distribution issues caused by feeder impedance difference and load unbalances. The power sharing behaviour under nonlinear filter inductor has not been investigated.

1.2.1.1 Nonlinear Characteristics of Filter Inductors

To explain the impact of filter inductor on system performance, nonlinear characteristic of filter inductor is firstly introduced. Power converter is an indispensable device in microgrids and filter is an essential component in power converter to provide high-quality electricity to local load or grid. In filter, inductor is a critical part whose magnetic core materials can highly affect hardware cost and operation performance of the converter.

There are two widely-used core materials in filter inductors, whose features are comparatively summarized in Table 1.1. Ferrite cores are widely used in converter filters because of the high linearity and low power loss under high frequency conditions. However, ferrite cores also have high cost and high sensitivity to temperature [17],[21], resulting in a high hardware cost and limited operation environment. Therefore, powder-core inductors are becoming alternative filter inductors due to their low cost [19],[25], high tolerance for temperature varying [19],[25] and high saturation flux density [15]-[22]. Although powder-core inductor is a preferable option as filter inductor considering all the performance factors, it has nonlinear behaviour because of the inherent soft-saturation characteristic of powder core, as shown in Fig. 1.3. The permeabilities of a ferrite core and a powder core are shown in Fig. 1.3 (a). It can be seen that ferrite core has hard-saturation characteristic,

which means that the permeability can almost keep at a constant value until magnetic field strength increases to the saturation point. Ferrite core can only work within the non-saturation region because the permeability will decrease sharply once the magnetic field strength went through the saturation point, which can result in system stability issues. Different from ferrite core, powder core has soft-saturation characteristic, which means that the permeability is reduced slowly as the magnetic field strength increases. Because of the soft-saturation characteristic, powder core normally has a wider working region than ferrite core [19]. However, the soft-saturation characteristic can also lead to issues in filter design, stability and power control performance. Fig. 1.3 (b) shows permeabilities of different powder cores. It can be seen that different powder materials can have different nonlinear characteristics, which can lead to potential power control issues among paralleled converters.

Table 1.1. Comparative analysis for different magnetic materials [10]

	Application [15]-[16]	Advantages [17]-[25]	Disadvantages [17]-[25]
Ferrite Magnetic Cores	• Filter inductor • High-frequency transformer	• High linear Degree • Small high-frequency loss	• High cost • Sensitive to temperature variation
Powder Magnetic Cores	• Filter inductor	• High saturation flux density • Good robustness to temperature variation • Small low-frequency loss • Low cost	• Soft-saturation nonlinearity

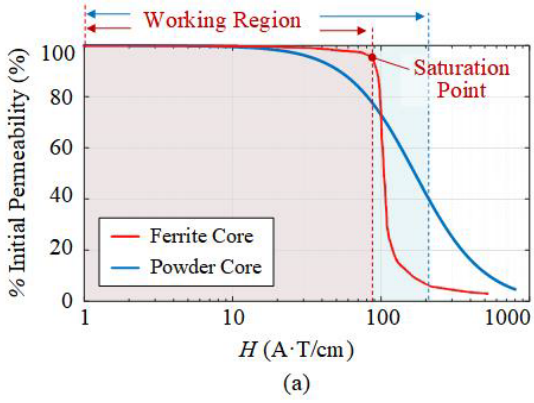

(a)

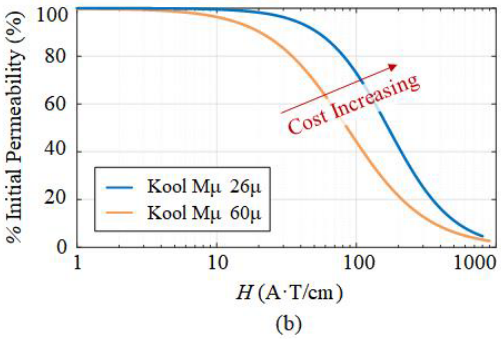

Fig. 1.3. Permeability behaviour of different materials [10]. (a) Ferrite core and powder core. (b) Different powder cores.

1.2.1.2 Impact of Nonlinear Filter Inductors on System Performance

With the increasing utilization of powder-core inductors, impacts of nonlinear behaviour of powder-core inductors have to be considered for filter design, converter controller design, stability analysis, etc. In fact, it has been paid more and more attention in grid-integrated converter design [18]-[20],[27]-[29]. In [27], the impact of nonlinear filter inductor is firstly investigated in a grid-integrated PV converter, where the nonlinear inductance is calculated by a self-learning algorithm to ensure the accurate current estimation. In [18], a *LCL* filter parameter optimization method is proposed for grid-integrated DG to improve system stability and power quality, where the influence of nonlinear filter inductor on resonant frequency is considered in filter design by including the nonlinear inductor model to the constraints of filter parameters. In [19], current harmonic characteristic under inductance varying is studied and a resonance control method is presented to minimize current harmonic. Reference [20] also analyzes the influence of powder-core inductor on current ripple, where a voltage calculation method is proposed to analyze the electrical behaviour of powder-core inductor. A voltage compensation method and filter inductor design method are further presented to perform satisfied current quality with powder-core inductor. In [28], a variable-structure inductance calculation mothed is proposed to analyze large-signal stability of grid-integrated converter. Then, an inductance-based impedance stability method is presented to study system stability under the whole inductance varying range. A direct digital controller is also developed based on the inductor model to solve the stability issue due to powder-core filter inductor. Reference [29] studies the impact of filter soft-saturation behaviour on output current of grid-integrated converter, where a robust current controller is provided to ensure low-harmonic current injection.

However, the aforementioned research tends to address the issues of nonlinear inductor in an individual converter. When it comes to microgrid with paralleled DGs, analysis method and controller design are different considering the interaction

between paralleled converters. Power sharing performance can be more complicated with consideration of the soft-saturation characteristic of power-core filter inductor, which is slightly addressed in previous research. Therefore, the first objective of this project is to ensure the desired power distribution performance of microgrids despite nonlinear filter inductors.

1.2.2. OPTIMIZATION ISSUES FOR EFFICIENCY AND COST

Operation efficiency is a key concern in power conversion system for long-term energy saving. Efficiency improvement methods of an individual converter have been paid numerous attention by modulator design [30]-[33], topologies design and passive component optimization [34]-[37], etc. However, there is very limited research on efficiency improvement challenge of microgrids.

In fact, the efficiency characteristic of microgrids is more complicated due to the different behaviours of paralleled DGs. However, it also provides room to improve the system efficiency at a system level, which can be divided into two categories. The first mothed is to dynamically change the amount of working DGs according to load profile. The theory behind this method is illustrated in Fig. 1.4, which plots efficiency curves of the system under different paralleled DGs numbers. It should be noticed that the system efficiency is higher with fewer converters activated under light load condition, instead of having all DGs working. Therefore, a sequential DG-activation method is proposed in [38] to reduce system power loss within light-load range. In [38], the number of working DGs is determined based on load profile, where only one DG is activated at first, then the second DG will be turned on once the first DG reaches its rating power, and so on. However, it should be noticed that the intersection points should be the optimum points to turn on next DG, as shown in Fig. 1.4, which is not the power rating points. To further improve system efficiency, [41] proposes a sweep algorithm to optimize the activation points of DGs under different load conditions, where system efficiency is significantly enhanced especially during light load condition.

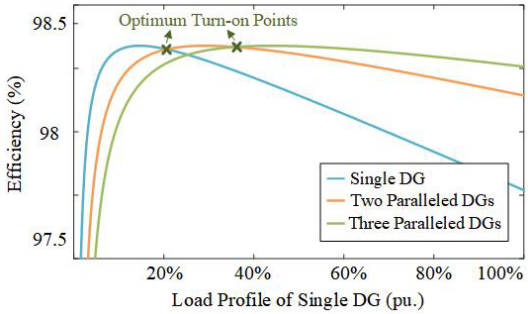

Fig. 1.4. System efficiency curves with different number of paralleled DGs.

However, different power loss characteristics of DGs are not considered in the aforementioned research. In fact, the power loss behaviours of DGs can be different because of the diversity of inverter type, lifetime, working condition, etc. Therefore, the second method to enhance system efficiency is to dynamically adjust power distribution performance according to power loss characteristics of different DGs [42]-[43],[48]. In [42], the efficiency of DC microgrids is improved by a hierarchical control strategy. Genetic algorithm is utilized at the tertiary level to calculate the power sharing references by solving the optimization problem. Then the power sharing references are achieved by virtual resistance method at the primary level, so that the optimum system efficiency is ensured. In [43], a smart controller is proposed based on a particle swarm optimization algorithm to capture the optimum efficiency point according to efficiency curves of inverters, where the power loss under light load can be reduced by the smart controller. However, centralized communication is needed in [42] and [43] in the optimization calculation progress, which will increase hardware cost and reduce system reliability because of the potential risk of data loss and time delay [44]-[47]. To avoid the drawbacks, reference [48] proposes a controller to achieve efficiency optimization with distributed communication instead of centralized communication links, which can ensure higher flexibility compared with centralized control methods. However, a dynamic consensus algorithm is used to optimize power distribution references in real time, which can increase the system computational burdens. Therefore, it is important to investigate the core relationship between system efficiency and power distribution ratio and develop a decentralized control method to improve system efficiency.

Apart from system efficiency, operation cost is another concern in microgrids. There are many researches about how to reduce system construction cost by sustainable energy planning [49], microgrid topology optimization [50], ESS sizing optimization [51], etc. However, the operation cost of microgrids is slightly concerned. In fact, due to the different cost characteristics of different DGs, system operation cost is related to power allocation among paralleled DGs. This offers the possibility to further reduce operation cost by adjusting power allocation. There are some centralized control methods that can achieve optimized dispatch, where load prediction and cost parameters of DGs are used in centralized power management center to decide the power allocation references [52]-[53]. However, the centralized controller relies on communication infrastructure which can increase hardware cost and reduce system flexibility. In order to deal with the drawback, decentralized control methods are proposed recently [54]-[57]. In [54], system operation cost is improved by dynamically adjusting droop parameters, so that the DG with less cost can provide more power. In [55], nonlinear droop controller is proposed to implement the economic dispatch, where the droop coefficients of each DG are calculated according to their own cost characteristics. Another nonlinear droop control strategy is proposed in [56] to minimize the system operation cost, where a two-stage particle swarm optimization method is used to generate the controller parameters. However, nonlinear controllers can be complex and difficult to be implemented in industry. A linear droop

control method is proposed in [57] to perform optimized cost operation according to the equal incremental cost principle. Furthermore, with the development of artificial intelligence techniques, intelligent controllers are also used to implement the economic power management of microgrids [58]-[60]. However, these intelligent controllers need enormous data and computationally intensive programs to execute.

Although the abovementioned works have developed many analysis and control methods to improve system efficiency and cost respectively, there is not much research about optimized dispatch in microgrids considering operation cost and system efficiency simultaneously. In fact, the system efficiency and operation cost can be highly coupled [61], which means that the optimization of system efficiency can deteriorate operation cost, and vice versa. Therefore, the second objective of this project is to solve the twofold optimization problem and develop a decentralized controller to perform the optimized power allocation in microgrids.

1.3. RESEARCH OBJECTIVES

Based on the aforementioned challenges, this project aims to enhance operation performance of AC microgrids by addressing the following research objectives:

(1) **Power sharing performance improvement considering nonlinear characteristics**

With the increasingly using of powder-core inductors, the impact of the inherent nonlinearity on power distribution performance needs to be addressed. This thesis investigates the impact and designs a local controller to mitigate the impact.

(2) **System efficiency improvement**

Although communication-based controllers have been presented to enhance efficiency of microgrids, the core relationship between power distribution and maximum system efficiency is slightly analyzed. This thesis reveals efficiency characteristics of microgrids and obtains the optimization conditions of capturing the maximum efficiency under different load conditions. A local controller is also developed to improve system efficiency according to the proposed optimization conditions.

(3) **System overall performance enhancement**

System efficiency and cost both can be improved by regulating power sharing. However, independent optimization of system efficiency or cost is not able to ensure overall performance optimization due to the coupling between them. This thesis addresses the twofold optimization for system efficiency and cost and proposes a decentralized controller to improve system overall performance.

1.4. THESIS OUTLINE

This thesis contains two parts: thesis report and selected publications. The relationship between these two parts is shown in Fig. 1.5.

Chapter 1 gives an introduction of the background and objectives of this research. Chapter 2 studies the impact of nonlinear inductors on power distribution behaviour and proposes a robust droop controller to reject the impact. Chapter 3 analyzes the efficiency characteristics of microgrids under different load profiles and presents a local controller to improve system efficiency. Chapter 4 analyzes the coupling behaviour of system efficiency and cost and develops a decentralized controller to improve system overall performance. Chapter 5 summarizes the thesis and gives the future work of the study.

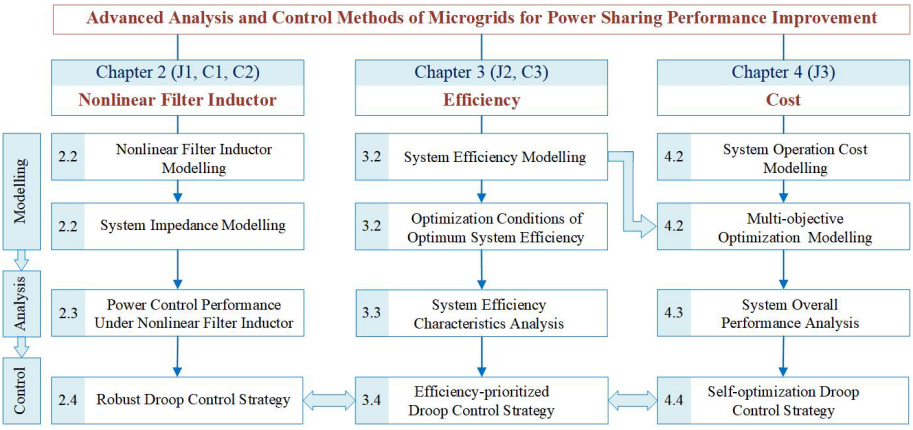

Fig. 1.5. Outline of the thesis.

1.5. LIST OF PUBLICATIONS

Publications related to the thesis are listed below.

Journal Papers

J1. **W. Yuan**, Y. Wang, D. Liu, F. Deng, and Z. Chen, "Impacts of inductor nonlinear characteristic in multiconverter microgrids: Modeling, analysis, and mitigation," *IEEE J. Emerg. Sel. Topics Power Electron.,* vol. 8, no. 4, pp. 3333-3347, Dec. 2020.

J2. **W. Yuan**, Y. Wang, D. Liu, F. Deng, and Z. Chen, "Efficiency-prioritized droop control strategy of AC microgrid," *IEEE J. Emerg. Sel. Topics Power Electron.,* vol. 9, no. 3, pp. 2936-2950, June 2021.

J3. **W. Yuan**, Y. Wang, and Z. Chen, "New perspectives on power control of AC microgrid considering operation cost and efficiency," *IEEE Trans. Power Systems,* vol. 36, no. 5, pp. 4844-4847, Sep. 2021.

Conference Papers

C1. **W. Yuan**, Y. Wang, D. Liu, F. Deng, and Z. Chen, "Robust droop control of AC microgrid against nonlinear characteristic of inductor," in *Proc. PEDG*, June 3-6, 2019, pp. 642-647.

C2. **W. Yuan**, Y. Wang, D. Liu, F. Deng, and Z. Chen, "Parameter estimator-based power control strategy of microgrid considering nonlinear inductor," in *Proc. APEC*, June 14-17, 2021, pp. 83-88.

C3. **W. Yuan**, Y. Wang, D. Liu, F. Deng, and Z. Chen, "Efficiency modelling and analysis of multi-bus microgrid with transmission network," in *Proc. ECCE Asia*, Nov. 29-Dec. 2, 2020, pp. 676-681.

Chapter 2. Power Sharing Performance of Microgrids Under Nonlinear Filter Inductors

2.1. ABSTRACT

Power sharing performance is important for system reliability, efficiency, cost, etc. However, it can be deteriorated by nonlinear powder-core filter inductors. In this chapter, model of nonlinear inductor is first built to present the soft-saturation behaviour of powder-core inductor. Then, impedance model of microgrid is presented to study the impact of inductor nonlinearity on power distribution behaviour. A robust droop controller is further designed to ensure desired power control performance with consideration of nonlinear filter inductors.

2.2. SYSTEM MODELLING CONSIDERING INDUCTOR NONLINEAR CHARACTERISTICS

2.2.1. SYSTEM DESCRIPTION

Fig. 2.1 shows circuit configuration of an AC microgrid, which can work either on islanded mode or grid-integrated mode. The DG consists of energy source, DC capacitor to stabilize voltage fluctuation from the energy source, inverter to transfer DC voltage to AC voltage, *LCL* filter to ensure the power quality and local controller to generate voltage reference and switch gate signals. Then the DGs are connected to the point of common coupling (PCC) through cable lines, supplying power to consumers or grid. In this thesis, all the research is based on this configuration in islanded mode. In islanded microgrids, droop controller is widely used to perform proportional power distribution without using communication links. With droop controller, the DG works as a voltage-source inverter (VSI) and can be modeled as a voltage-controlled source with a series-connected impedance by Thevenin Equivalent Circuit modelling.

Assuming inductive line impedance between DG and PPC [62], the classical droop control [62]-[63] is given as (2-1)-(2-2).

$$\omega_i^* = \omega_0 - m_i P_i \tag{2-1}$$

$$V_i^* = V_0 - n_i Q_i \tag{2-2}$$

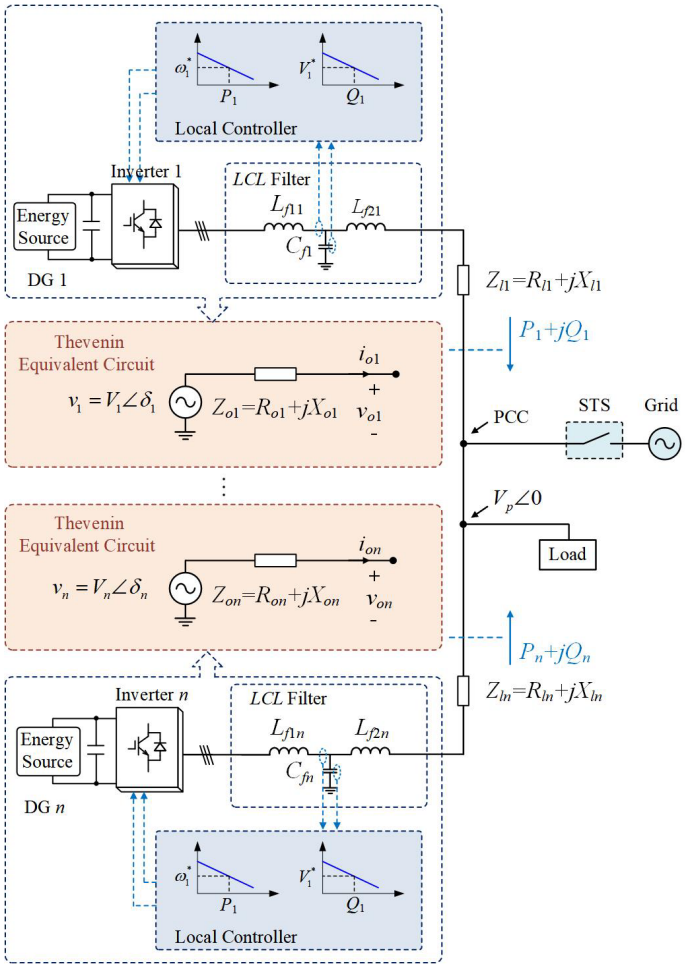

Fig. 2.1. Circuit configuration of AC microgrid [10].

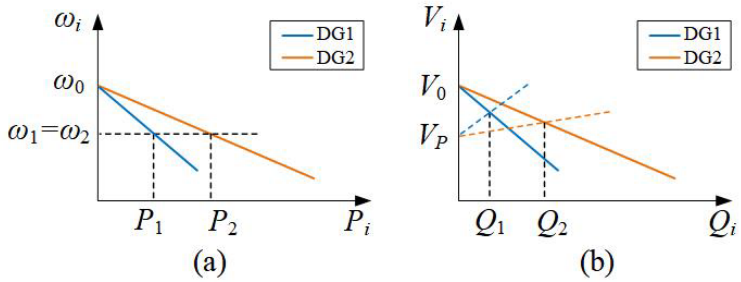

Fig. 2.2. Classical droop control curves. (a) *P*-ω curve. (b) *Q*-*V* curve.

where V_i^* and ω_i^* are voltage amplitude and angular frequency references of the i-th DG. V_0 and ω_0 are voltage amplitude and angular frequency of DG without load. m_i and n_i are droop coefficients that are given as (2-3) and (2-4) in classical droop control strategy.

$$m_i = \left(\omega_{\max} - \omega_{\min}\right) / P_{\max i} \tag{2-3}$$

$$n_i = \left(V_{\max} - V_{\min}\right) / Q_{\max i} \tag{2-4}$$

where $V_{\max}$ and $V_{\min}$ are allowable range of voltage amplitude variation, $\omega_{\max}$ and $\omega_{\min}$ are allowable range of voltage angular frequency variation. $P_{\max i}$ and $Q_{\max i}$ are active and reactive power ratings, respectively.

Fig. 2.2 shows the control curves of classical droop controller. Fig. 2.2 (a) shows the active power (P)- angular frequency (ω) curve which is plotted according to (2-1). Taking two DGs as an example, (2-5) must be ensured in the steady state. Then (2-6) can be obtained by combining (2-1), (2-3) and (2-5), meaning that the active power can be distributed proportionally by traditional droop controller. Reactive power (Q)- voltage amplitude (V) curves are shown in Fig. 2.2 (b) as the solid lines which are plotted according to (2-2). Assuming inductive line impedance between DG and PPC [62], the dotted lines in Fig. 2.2 (b) show the terminal characteristics of DGs which is given as (2-7), where V_p is the PCC voltage amplitude, X_{oi} is the equivalent output reactance of DG, X_{li} is the cable reactance from DG to PCC. The operation point of reactive power is actually the intersection of droop control curve and terminal characteristic curve, as shown in Fig. 2.2 (b). The reactive power is shared as (2-8) under traditional droop controller [10], which shows that reactive power distribution performance depends on output reactance, cable reactance and Q-V droop coefficient.

$$\omega_1 = \omega_2 \tag{2-5}$$

$$\frac{P_1}{P_2} = \frac{m_2}{m_1} = \frac{P_{\max 1}}{P_{\max 2}} \tag{2-6}$$

$$V_i = V_p + \frac{X_{oi} + X_{li}}{V_p} Q_i \tag{2-7}$$

$$\frac{Q_1}{Q_2} = \frac{X_{o2} + X_{l2} + n_2 V_p}{X_{o1} + X_{l1} + n_1 V_p} \tag{2-8}$$

In fact, the reactive power distribution error due to different cable impedances has been dealt with in previous works [4]-[14]. However, the impact of nonlinear filter inductor is merely considered, which will be elaborated in Section 2.3.

2.2.2. NONLINEAR INDUCTOR MODELLING

The nonlinear inductor model is built in this section to study nonlinear behaviour of powder-core filter inductor caused by soft-saturation characteristic.

Fig. 2.3 shows diagram of an inductor with magnetic core. The voltage across an inductor u_L can be given as (2-9) based on electrical feature or (2-10) based on magnetic feature [64].

$$u_L = L\left(i_L\right)\frac{di_L}{dt}$$

$$u_L = N\frac{d\Phi}{dt} \tag{2-10}$$

where L is inductance which is current-dependent for powder-core inductor. i_L is inductor current as shown in Fig. 2.3. N is number of coil turns. Φ is magnetic flux through the coil. Φ is defined as (2-11) where B is magnetic flux density that is assumed to be uniform over area A [28],[64].

$$\Phi = BA \tag{2-11}$$

B is given as (2-12).

$$B=\mu\left(H\right)H \tag{2-12}$$

where μ and H are magnetic permeability and magnetic field strength of inductor core, respectively. For powder core, μ is a nonlinear formula of H as (2-13) [15].

$$\mu=\left(a+bH+cH^2+dH^3+eH^4\right)\cdot\mu_i \tag{2-13}$$

where μ_i is the initial permeability of powder core. a, b, c, d and e are coefficients that are different for different cores and can be found in datasheet [15]. H is given as (2-14) according to Ampere's circuital law [64].

$$H = \frac{Ni_L}{l} \tag{2-14}$$

where l is the length of a toroid.

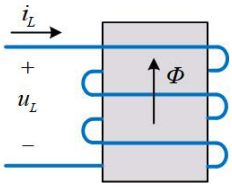

Fig. 2.3. The diagram of an inductor with core [10].

In order to obtain the relationship between μ and i_L, magnetic permeability is derived as (2-15) by combining (2-13) and (2-14) [10]

$$\mu'(i_L) = a' + b'i_L + c'i_L^2 + d'i_L^3 + e'i_L^4 \tag{2-15}$$

where

$$a'=a\mu_i,\ b'=\frac{b\mu_i N}{l},\ c'=\frac{c\mu_i N^2}{l^2},\ d'=\frac{d\mu_i N^3}{l^3},\ e'=\frac{e\mu_i N^4}{l^4}$$

Inductance of the powder-core inductor can be derived as (2-16) by combining (2-9) -(2-15) [10].

$$L(i_L) = N\frac{d\Phi}{di_L} = \frac{AN^2}{l}\left[\mu'(i_L) + i_L\frac{d\mu'(i_L)}{di_L}\right] = f(i_L) \tag{2-16}$$

Then assuming the inductor current as $i_L=I_m\sin(\omega t)$, the average inductance is obtained as (2-17) [10].

$$L_{avg} = \frac{1}{T}\int_0^T L(i_L)dt = a_{avg} + c_{avg}I_m^2 + e_{avg}I_m^4 = g(I_m) \tag{2-17}$$

where

$$a_{avg} = \frac{a\mu_i AN^2}{l},\ c_{avg} = \frac{3c\mu_i AN^4}{2l^3},\ e_{avg} = \frac{15e\mu_i AN^6}{8l^5}$$

In fact, the inductance used in previous work is an instantaneous value which defined as (2-18) [10].

$$L_{nom} = \lim_{i_L\to 0} L \tag{2-18}$$

Fig. 2.4 shows the powder-core inductance curves based on (2-17) and datasheet[67]-[68], where the practical inductance is changed as current increasing. Besides, there are different soft-saturation nonlinear characteristics in different

powder-core inductors. Note that the inductance will converge to a small positive value with inductor current increasing. However, in practical application, the filter inductor current is limited because of the converter current limitation, which also limits the inductance varying range as shown in Fig. 2.4.

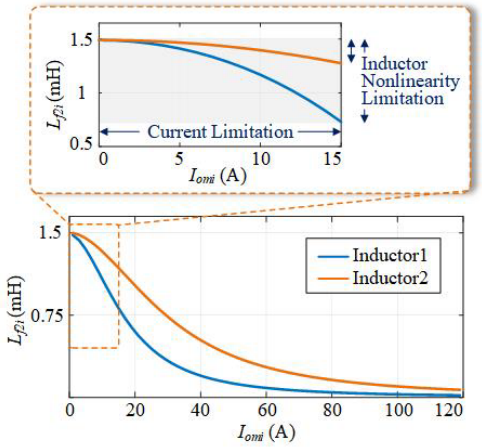

Fig. 2.4. Inductance curves of different powder-core inductors [10].

2.2.3. IMPEDANCE MODELLING OF MICROGRIDS CONSIDERING NONLINEAR INDUCTOR

The power sharing behaviour under nonlinear inductor is merely investigated in previous works, which is studied in this project. To reveal the influence of powder-core inductor on power distribution, system impedance model under power-core inductors is firstly built.

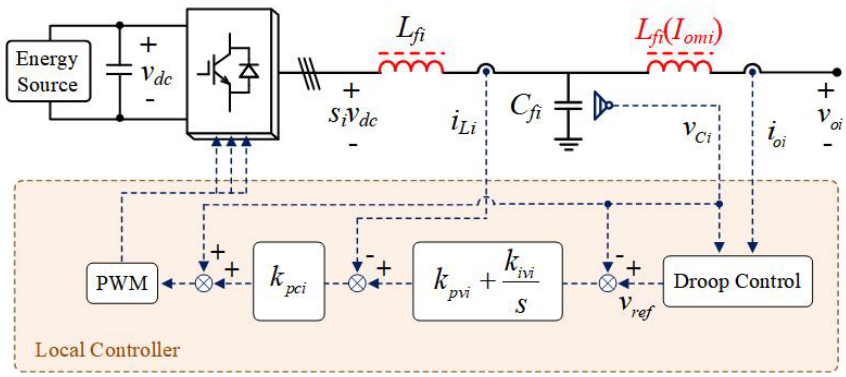

Fig. 2.5. The inverter configuration with local droop controller [10].

The inverter configuration is shown in Fig. 2.5, where dynamic differential equations of the converter are given as (2-19) [10].

$$\begin{cases} L_{f1i}\dfrac{di_{Li}}{dt} = s_i v_{dc} - v_{Ci} \\ C_{fi}\dfrac{dv_C}{dt} = i_{Li} - i_{oi} \\ L_{f2i}\dfrac{di_o}{dt} = v_{Ci} - v_{oi} \end{cases} \tag{2-19}$$

where s_i is a signal variable (1, 0 or -1) depending on the turn-on/off state of switches. The average open-loop voltage dynamic is presented as (2-20) [65]-[66].

$$\left\langle s_i v_{dc} \right\rangle = L_{f1i}C_{fi}\frac{d^2\left\langle v_{oi}\right\rangle}{dt} + \left\langle v_{oi}\right\rangle + L_{f1i}L_{f2i}C_{fi}\frac{d^3\left\langle i_{oi}\right\rangle}{dt} + L_{f1i}\frac{d\left\langle i_{oi}\right\rangle}{dt} + L_{f2i}\frac{d\left\langle i_{oi}\right\rangle}{dt} \tag{2-20}$$

where $\langle\ \rangle$ means average value over one switching time period.

In a VSI, the dual-loop controller is usually used as Fig. 2.5. Then the voltage dynamic of dual-loop controller is presented as (2-21) [10], [66].

$$\left\langle s_i v_{dc} \right\rangle = \left\langle v_{refi}\right\rangle + k_{pci}\left(k_{pvi}\left(\left\langle v_{refi}\right\rangle - \left\langle v_{Ci}\right\rangle\right) + k_{ivi}\int\left(\left\langle v_{refi}\right\rangle - \left\langle v_{Ci}\right\rangle\right)dt - \left\langle i_{Li}\right\rangle\right) \tag{2-21}$$

where v_{refi} is output voltage reference. k_{pvi} and k_{ivi} are proportional and integral gains of outer voltage-loop control. k_{pci} is the proportional gain of inter current-loop control.

The inverter output voltage is then derived as (2-22) by combining (2-19)-(2-21) [10].

$$V_{oi}(s) = G_i(s)V_{refi}(s) - Z_{oi}(s)I_{oi}(s) \tag{2-22}$$

where $G_i(s)$ and $Z_{oi}(s)$ are voltage gain and output impedance respectively, which are presented as (2-23) and (2-24) [10].

$$G_i(s) = \frac{\left(1 + k_{pci}k_{pvi}\right)s + k_{pci}k_{ivi}}{L_{f1i}C_{fi}s^3 + k_{pci}C_{fi}s^2 + \left(1 + k_{pci}k_{pvi}\right)s + k_{pci}k_{ivi}} \tag{2-23}$$

$$Z_{oi}\left(I_{omi},s\right)=\frac{\begin{array}{l}L_{f1i}L_{f2i}\left(I_{omi}\right)C_{fi}s^4+k_{pci}L_{f2i}\left(I_{omi}\right)C_{fi}s^3\\+\left(k_{pci}k_{pvi}L_{f2i}\left(I_{omi}\right)+L_{f1i}+L_{f2i}\left(I_{omi}\right)\right)s^2+\left(k_{pci}k_{ivi}L_{f2i}\left(I_{omi}\right)+k_{pci}\right)s\end{array}}{L_{f1i}C_{fi}s^3+k_{pci}C_{fi}s^2+\left(1+k_{pci}k_{pvi}\right)s+k_{pci}k_{ivi}} \tag{2-24}$$

Substituting $s=j\omega_0$ into (2-24), the output reactance is given as (2-25) [10].

$$X_{oi}\left(I_{omi}\right)=\mathrm{Im}\left(Z_{oi}\left(I_{omi},s=j\omega_0\right)\right)=h\left(L_{f2i}\left(I_{omi}\right)\right)=h'\left(I_{omi}\right) \tag{2-25}$$

where I_{omi} is the amplitude of output current i_{oi}. L_{f2i} (I_{omi}) is the current-depend nonlinear inductance of filter inductor which is given by (2-17). Equation (2-25) shows that the output impedance becomes nonlinear and current-dependent because of the nonlinear inductor L_{f2i}.

2.3. IMPACTS OF NONLINEAR INDUCTOR ON POWER SHARING PERFORMANCE

To study the impact of nonlinear filter inductor on reactive power distribution behaviour, a microgrid with two DGs of same power rating inverters but different *LCL* filters is exemplified. And the same cable impedance is assumed in the analysis to avoid the influence of the mismatched cable impedances.

Under nonlinear filter inductors, the reactive-power-distribution ratio can be obtained as (2-26) by combining (2-8) and (2-25). Equation (2-26) shows that the reactive-power-distribution ratio is nonlinear and current-dependent with consideration of nonlinear filter inductors. Fig. 2.6 shows the role of nonlinear filter inductor in the causation of reactive power distribution error. Fig. 2.6 (a) shows the nonlinear characteristic of powder-core filter inductor according to (2-17), which is caused by soft-saturation behaviour of powder core as analyzed in Section 2.2.2. Fig. 2.6 (b) shows the equivalent output reactance of DGs. The output reactance has the same behaviour as filter inductance, which is current-dependent and nonlinear. Fig. 2.6 (c) shows the reactive-power-distribution ratio under powder-core filter inductors. Fig. 2.6 shows that the nonlinear behaviour of power-core filter inductors results in the nonlinear output reactance of DGs, which further influences the reactive power distribution.

$$\frac{Q_1}{Q_2}=\frac{X_{o2}\left(I_{om2}\right)+X_{l2}+n_2V_p}{X_{o1}\left(I_{om1}\right)+X_{l1}+n_1V_p} \tag{2-26}$$

Fig. 2.7 shows the operation points variation of DGs with increasing load profiles under traditional droop controller and nonlinear filter inductors, giving another insight into the impact of nonlinear inductors on reactive power distribution. The black line is the droop control curve, which is the same for two DGs since the two DGs are of

same rating power. The blue line is external characteristic line of DG1 and the orange line is external characteristic curve of DG2, which are plotted according to (2-7). And the operation point is the intersection point of droop control curve and external characteristic curve. Fig. 2.7 (a) shows that the reactive power is shared equally under light load because the initial inductances of two filter inductors are the same. However, with the load increasing, the external characteristic curves of DGs rotate, leading to the variation of operation points, as shown in Fig. 2.7 (b) and Fig. 2.7 (c). Since the filter inductors are of different nonlinearities, the output reactances of two DGs change differently, leading to the external characteristic curves rotating differently. In addition, the reactive power sharing error becomes bigger with load profile increases because the filter inductance mismatch becomes bigger, which aligns with the theory analysis shown in Fig. 2.6.

It needs to be noted that different from the impact of mismatched cable impedance, the impact of powder-core filter inductors is current-dependent and nonlinear, which cannot be mitigated by the existing droop control methods. Therefore, a robust droop controller is designed in Section 2.4 to enhance reactive power control performance under nonlinear inductors.

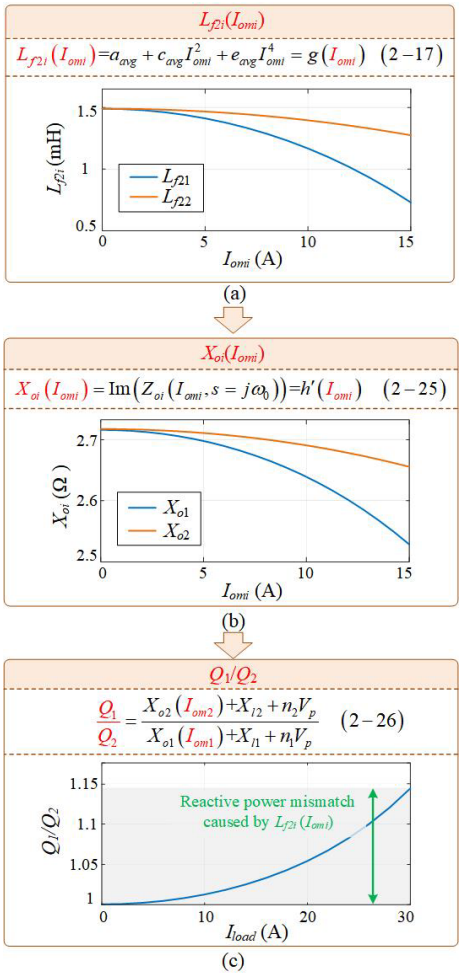

Fig. 2.6. Reactive power sharing characteristic under nonlinear filter inductors [10].

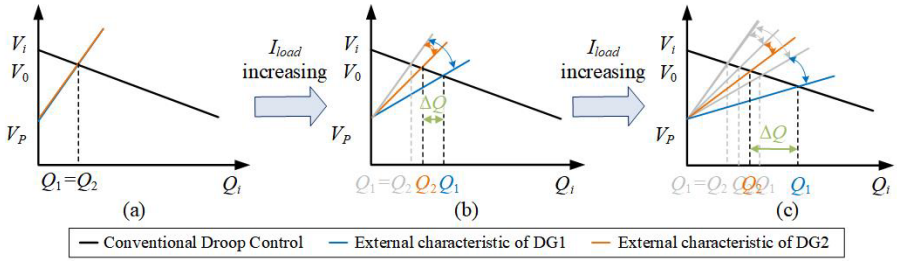

Fig. 2.7. Operation points variation with increasing load profiles.

2.4. THE PROPOSED ROBUST DROOP CONTROLLER AGAINST INDUCTOR NONLINEAR CHARACTERISTICS

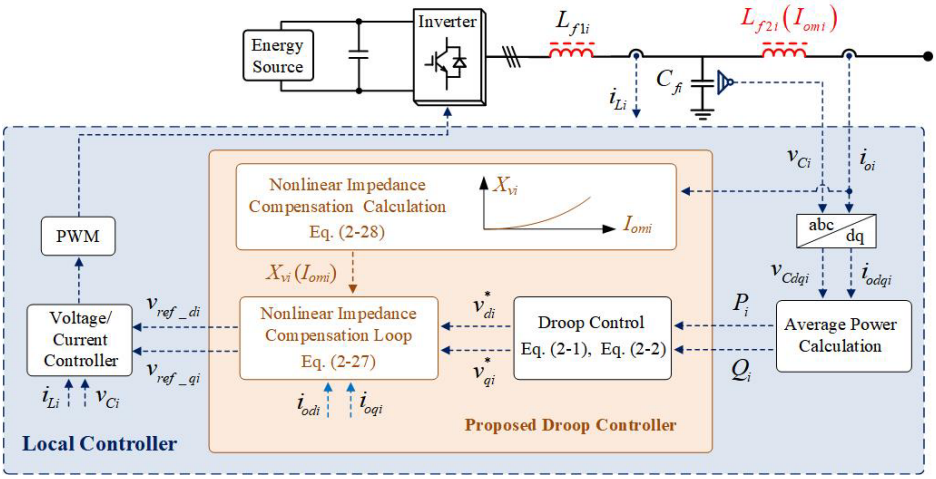

Fig. 2.8. Control diagram of proposed robust droop control method [10].

A robust droop controller is presented to enhance reactive power control against nonlinear filter inductors, as shown in Fig. 2.8. The filter voltage and current are measured to calculate the output P and Q, as the input signals of the controller. In the proposed controller, the voltage reference is firstly calculated according to (2-1) and (2-2) then transferred to d-q frame. Then, the final voltage references are retuned as (2-27) by a nonlinear impedance compensation as (2-28) [10].

$$\begin{cases} v_{ref\_di} = v_{di}^* + X_{vi}(I_{omi}) i_{oqi} \\ v_{ref\_qi} = v_{qi}^* - X_{vi}(I_{omi}) i_{odi} \end{cases} \tag{2-27}$$

$$X_{vi}(I_{omi}) = X_{oi}^* - X_{oi}(I_{omi}) \tag{2-28}$$

where

$$X_{oi}^* = \frac{k}{Q_{\max i}} \tag{2-29}$$

where v_{di}^* and v_{qi}^* are original voltage references obtained from traditional droop controller in d-q frame, i_{odi} and i_{oqi} are output current measurement in d-q frame. v_{ref_di} and v_{ref_qi} are final voltage references which are returned by nonlinear impedance compensation and sent to voltage/current dual-loop controller. X_{vi} (I_{omi}) is the proposed virtual impedance compensation, which is calculated according to

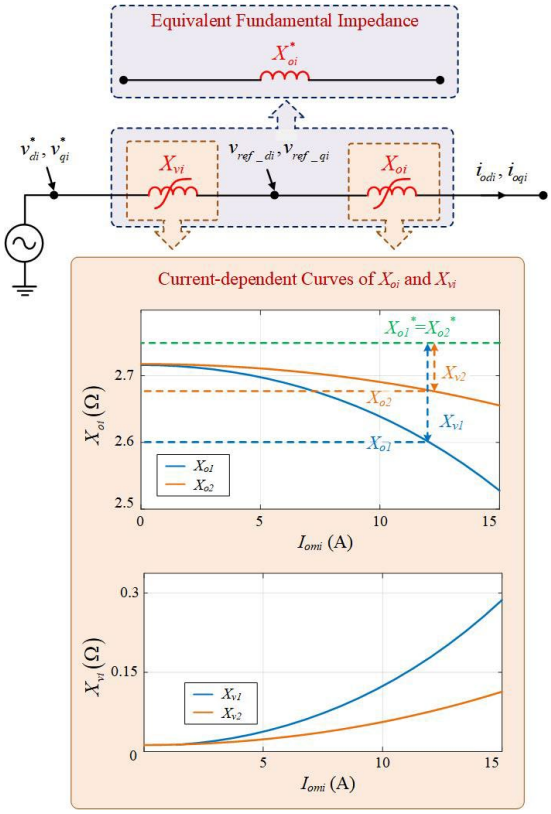

Fig. 2.9. Equivalent impedance of DG with nonlinear impedance compensation [10].

the nonlinear output impedance X_{oi} (I_{omi}). X_{oi}^* is the equivalent impedance which is a joint result of the actual output impedance and the virtual impedance compensation. k is a constant which is equal for all DGs.

Fig. 2.9 shows Thevenin equivalent circuit of a DG under the proposed impedance compensation. The principle of this controller is to generate a current-dependent impedance compensation, to make up the impedance variation caused by nonlinear filter inductor and lead to a constant equivalent output impedance. Then the reactive-power-distribution ratio under reshaped impedance is given as (2-30) [10].

$$\frac{Q_1}{Q_2}=\frac{X_{o2}^*+X_{l2}+n_2V_p}{X_{o1}^*+X_{l1}+n_1V_p} \tag{2-30}$$

Since the mismatch issue caused by cable impedance has been addressed by previous works [4]-[14], X_{li} in (2-30) can be assumed as power-rating related. At the same time, since X_{oi}^* and n_i are both designed as power-rating related, (2-31) can be

ensured, meaning that the reactive power is distributed proportionally under the proposed controller [10].

$$\frac{Q_1}{Q_2} = \frac{Q_{\max 1}}{Q_{\max 2}} \tag{2-31}$$

2.5. SIMULATION AND EXPERIMENTAL VALIDATION

2.5.1. SIMULATION VALIDATION

To validate the reactive power distribution of designed robust droop controller, simulation cases are executed in a two-DG AC microgrid in MATLAB/ SIMULINK. Fig. 2.10 shows the circuit of the exemplified microgrid. Simulation parameters are listed in Table 2.1. In the simulation, two powder-core inductors with different nonlinear characteristics as shown in Fig. 2.10 are used as filter inductors.

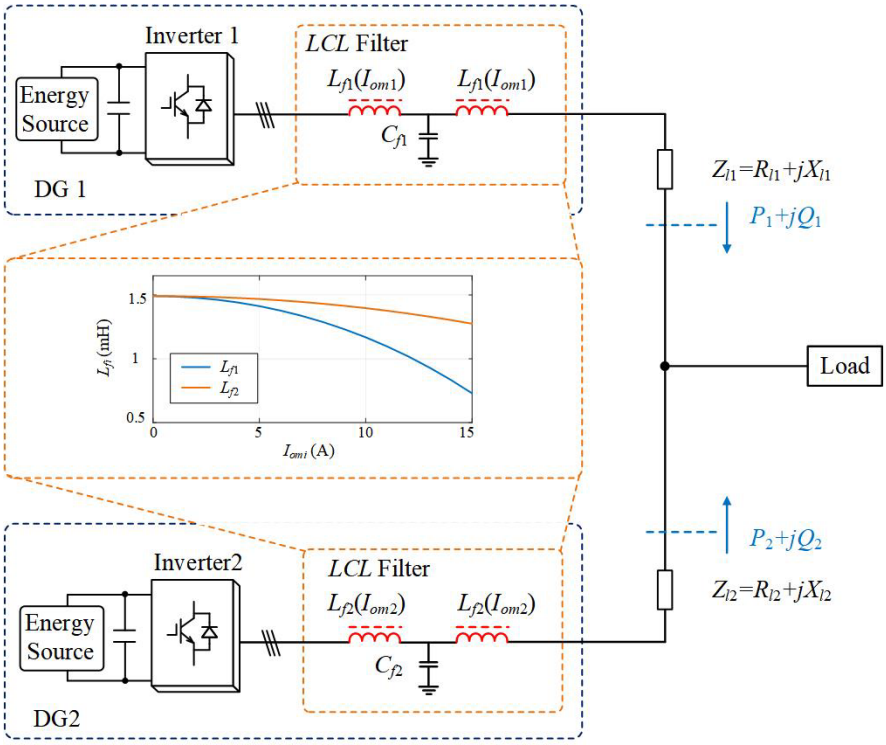

Fig. 2.10. Circuit configuration of the simulation test.

Table 2.1. Simulation Parameters [10]

Filter Inductor Parameters			
	L_{f1} [67]		L_{f2} [68]
Manufacturer	MAGNETICS		MAGNETICS
Part number	Kool Mμ 00K6527E026		Kool Mμ 00K160LE026
Initial permeability	26μ		26μ
Nominal inductance	L_{f1_nom}=1.5mH		L_{f2_nom}=1.5mH
Circuit Parameters			
DC voltage	500V	Line impedance	Z_{l1}=(0.01+j0.31) Ω
Filter parameters	C_{f1}=C_{f2}=25μF		Z_{l2}=(0.01+j0.31) Ω
Control Parameters			
Droop coefficients	Case I	m_1= m_2=6e-5, n_1= n_2=6e-4	
	Case II	m_1= 6e-5, m_2= 1.2e-4, n_1=6e-4, n_2=1.2e-3	
Impedance compensation coefficient		k=3.5e4	
Switching frequency		f_{sw1}=f_{sw2} =10kHz	

Case I: DGs with same power rating

In this case, two same-power-rating DGs are used to validate the proposed controller. To test the performance under the whole load profile, the load profile is changed from 40% to 60% of system rating at 0.6s, and from 60% to 80% of system rating at 1.2s.

Fig. 2.11 shows the power distribution with traditional droop controller under nonlinear filter inductors. Although accurate active power distribution is performed, the reactive power distribution is deteriorated because of the nonlinear filter inductors. In addition, since the filter inductance difference becomes bigger and bigger as load increases, the reactive power distribution error becomes more and more serious, which aligns with the theoretical analysis in Section 2.3.

Fig. 2.12 shows the simulation results with proposed droop controller, The power distribution performance is shown in Fig. 2.12 (a) and (b). Fig. 2.12 (c) shows the impedance compensation values which are calculated adaptively under different load profiles, to deal with the impacts caused by current-dependent filter inductors. Comparing Fig. 2.11 (b) and Fig. 2.12 (b), the proposed controller can mitigate the impact of nonlinear filter inductors and perform required reactive power distribution.

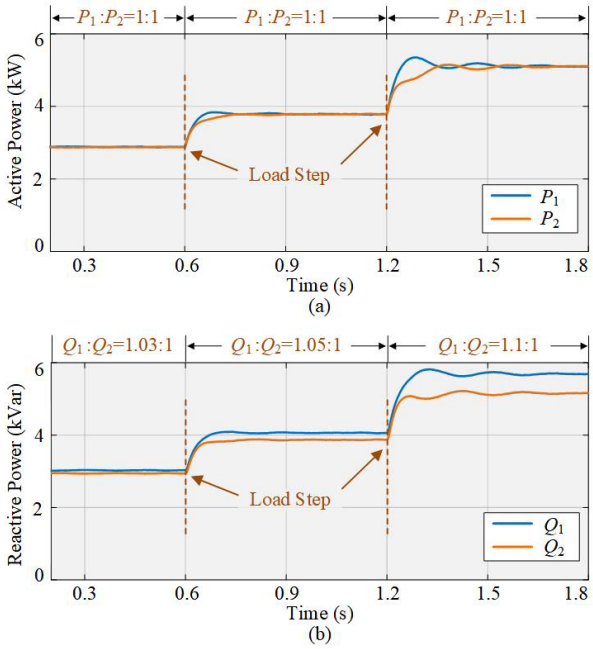

Fig. 2.11. Simulation results under traditional droop controller in case I [10]. (a) Active power. (b) Reactive power.

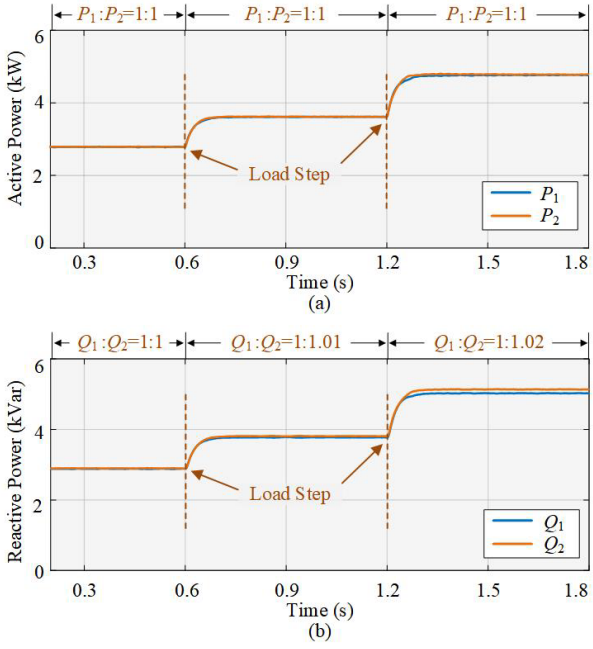

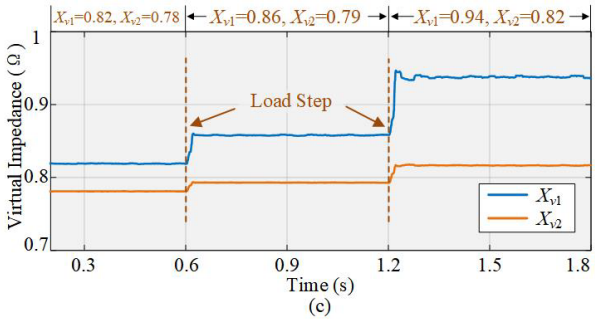

Fig. 2.12. Simulation results under proposed droop controller in case I [10]. (a) Active power. (b) Reactive power. (c) Nonlinear impedance compensation.

Case II: DGs with different power rating

In this case, two DGs of different power ratings are used, where S_{max1}:S_{max2}=2:1. The same load profile as case I is executed in this case. The power distribution results under traditional droop controller are shown in Fig. 2.13, where the reactive power distribution accuracy is deteriorated. The power distribution results under the proposed controller are shown in Fig. 2.14 (a) and (b). Fig. 2.14 (c) shows the impedance compensation term which is dynamically tuned according to nonlinear filter inductances. Fig. 2.14 shows that the proposed controller can perform proportional power distribution against the impacts of nonlinear filter inductors.

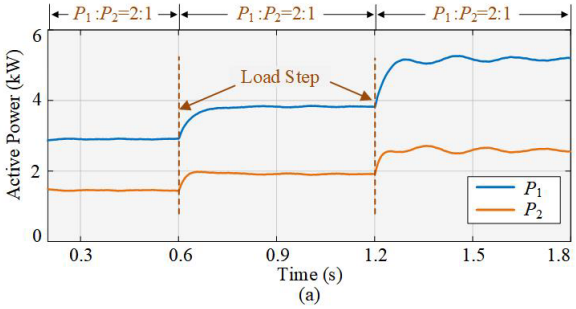

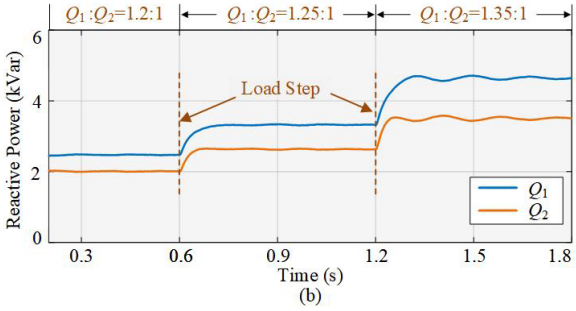

Fig. 2.13. Simulation results under traditional droop controller in case II [10]. (a) Active power. (b) Reactive power.

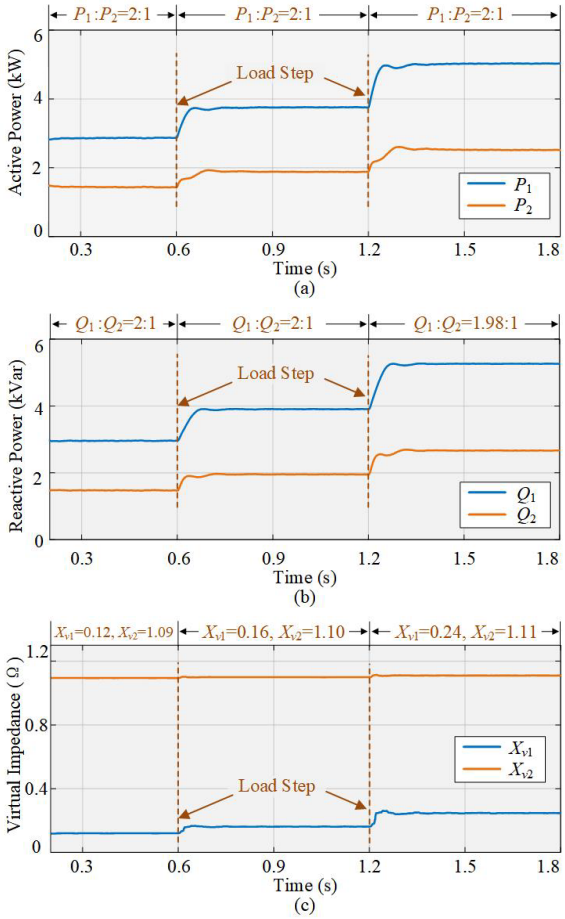

Fig. 2.14. Simulation results under proposed droop controller in case II [10]. (a) Active power. (b) Reactive power. (c) Nonlinear impedance compensation.

2.5.2. EXPERIMENTAL VALIDATION

To further test designed controller, experiment cases are executed in a scaled-down two-DG microgrid. Fig. 2.15 shows the experimental setup which consists of DC source, inverters, sampling circuit and *LCL* filters. dSPACE 1006 is used to control the setup. Experimental parameters are listed in Table 2.2. In the experiments, different nonlinear inductors are used in *LCL* filters. The practical inductance data is measured by Precision Magnetics Analyzer 3260B and shown in Fig. 2.16, where the filter inductance of inverter 1 reduces obviously as current increasing while the filter inductance of inverter 2 has almost no variation within current rating limitation.

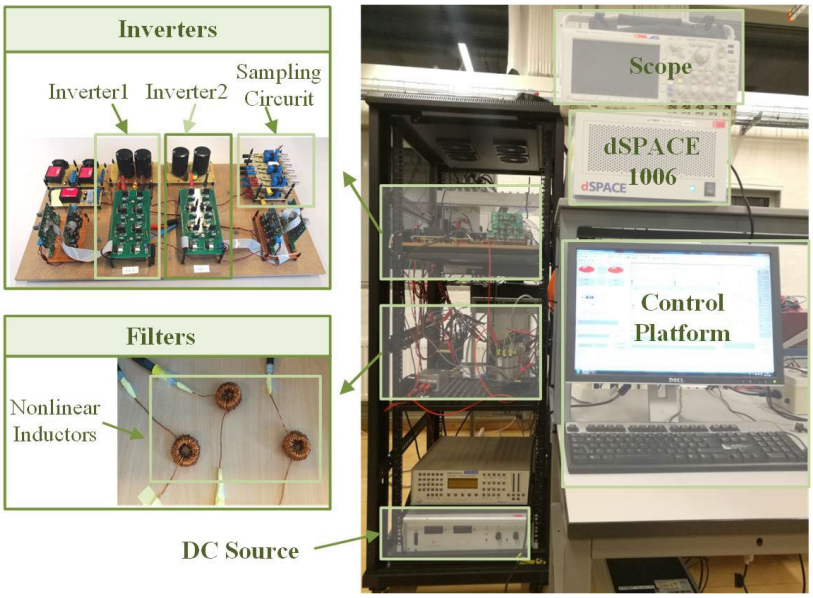

Fig. 2.15. Experimental setup [10].

Table 2.2. Experimental Parameters [10]

Circuit Parameters			
DC voltage	200V	Line impedance	Z_{l1}=(0.01+j0.56) Ω
Filter parameters	C_{f1}=C_{f2}=25μF		Z_{l2}=(0.01+j0.56) Ω
Control Parameters			
Droop coefficients		m_1= m_2=6e-5, n_1= n_2=6e-4	
Impedance compensation coefficient		k=3.5e4	
Switching frequency		f_{sw1}=f_{sw2} =10kHz	

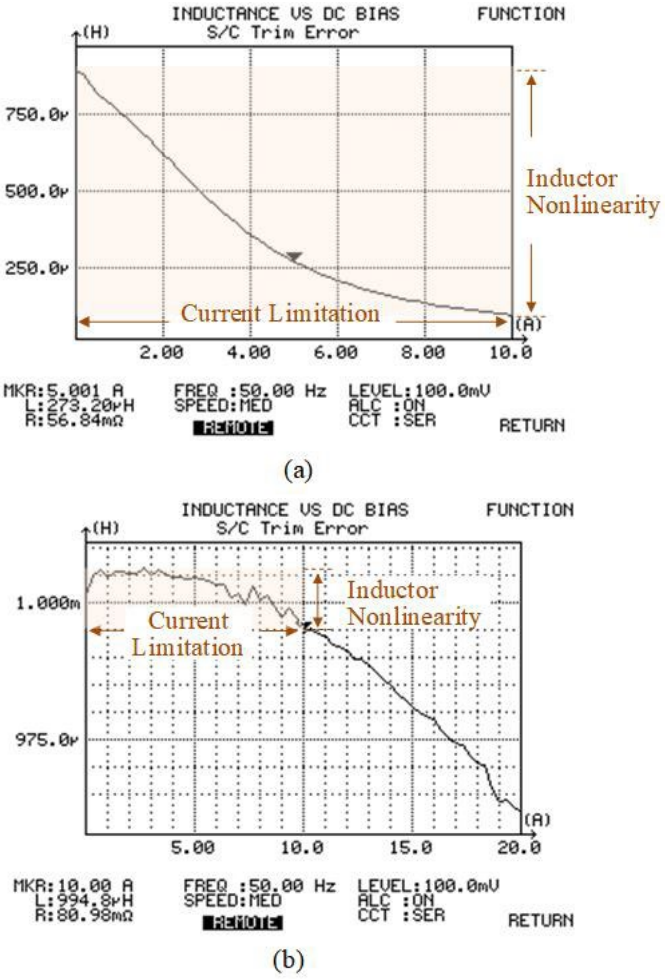

Fig. 2.16. Filter inductance measurements of two inverters [10]. (a) Filter inductance of inverter 1. (b) Filter inductance of inverter 2.

Fig. 2.17 shows phase-A currents of the two inverters under traditional droop controller. The traditional droop controller cannot ensure the desired power distribution result under nonlinear filter inductors. And the power sharing error is current-dependent because of the impacts caused by nonlinear filter inductors, which aligns with the analysis in Section 2.3. Fig. 2.18 shows phase-A currents of the two inverters under the proposed controller. Experiment results show that once the proposed controller is enabled, the power is equally distributed, against the impacts of nonlinear filter inductors.

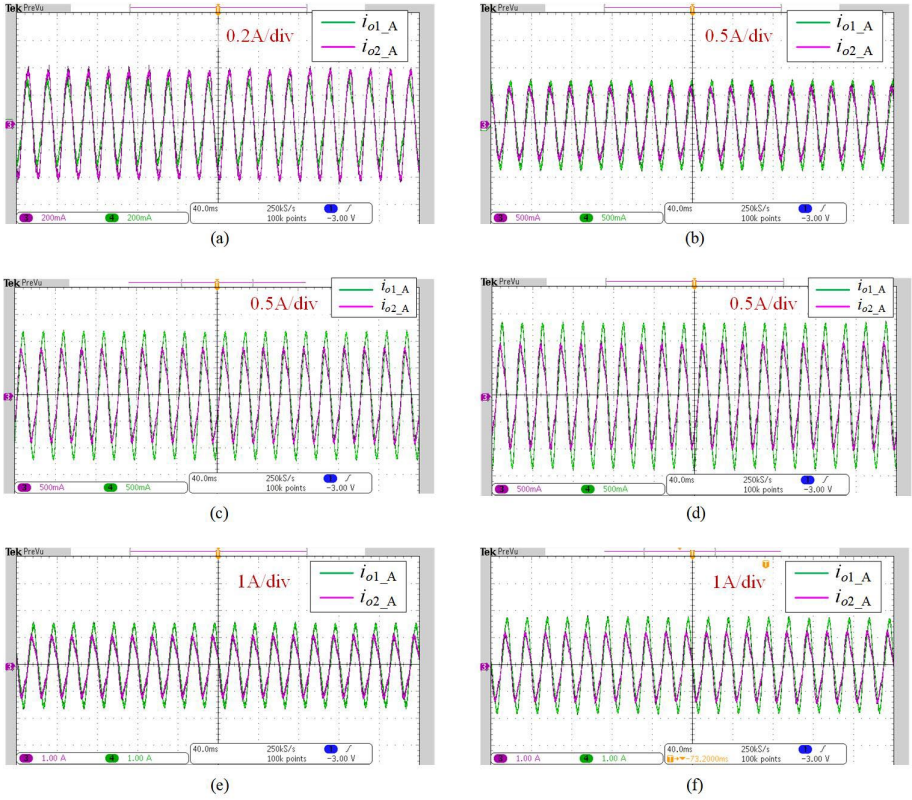

Fig. 2.17. Phase-A currents of inverters under traditional droop controller with increasing current reference [10]. (a) Current reference = 0.38A. (b) Current reference = 0.7A. (c) Current reference = 1A. (d) Current reference = 1.1A. (e) Current reference = 1.25A. (f) Current reference = 1.5A.

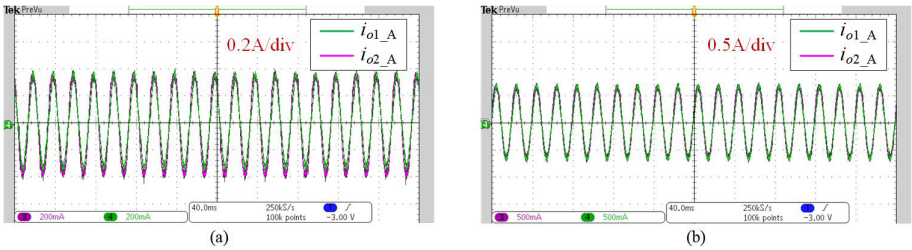

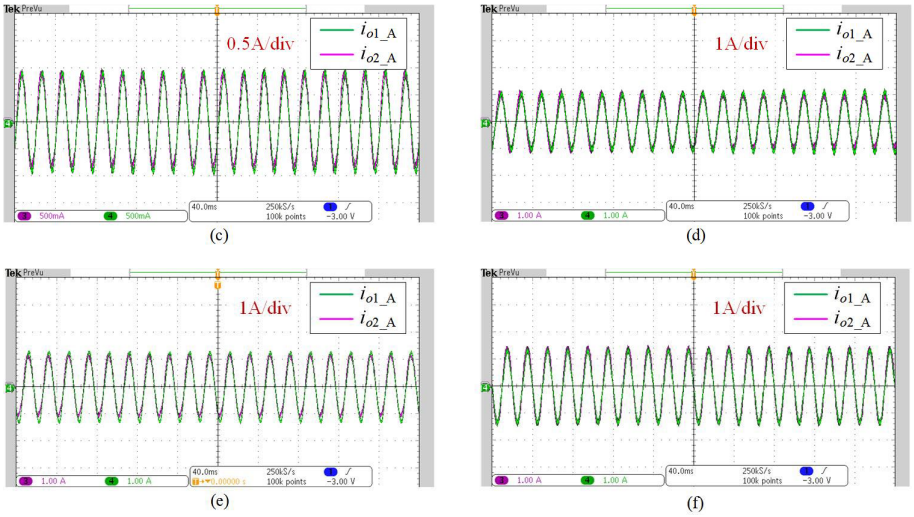

Fig. 2.18. Phase-A currents of inverters under proposed controller with increasing current reference [10]. (a) Current reference = 0.38A. (b) Current reference = 0.7A. (c) Current reference = 1A. (d) Current reference = 1.1A. (e) Current reference = 1.25A. (f) Current reference = 1.5A.

2.6. SUMMARY

This chapter presents the soft-saturation characteristic of powder-core inductors and investigates the impacts of powder-core filter inductors on power distribution performance. Inductor modelling is first established to study the nonlinear behaviours of powder-core filter inductors. System impedance model is then built to investigate the nonlinear reactive power mismatch caused by nonlinear filter inductors. A robust droop controller is further designed to reject the impact of nonlinear inductors, ensuring desired power distribution performance under cost-effective powder-core filter inductors. Simulation and experimental results show that the system can achieve desired power distribution under the proposed controller with immunity to nonlinear filter inductors, which means that the system can perform satisfying power distribution in a cost-effective way.

Chapter 3. Power Sharing Performance of Microgrids for System Efficiency Improvement

3.1. ABSTRACT

System efficiency is an important concern in microgrids, which is relevant to power sharing performance. However, the core connection between power distribution and system efficiency is slightly addressed. In this chapter, system efficiency optimization model is established and optimum conditions are obtained by Lagrange Multiplier Method. An efficiency-prioritized droop controller is further presented to improve system efficiency without using communication facilities.

3.2. EFFICIENCY MODELLING OF MICROGRIDS

3.2.1. SYSTEM DESCRIPTION AND PROBLEM FORMULATION

Under the traditional droop controller together with kinds of reactive power sharing methods, proportional power sharing can be performed as analyzed in Chapter 2. However, it might not be the optimal power sharing strategy for system efficiency improvement, which will be explained in this section. Note that the power loss of network is not considered in this thesis since cable distance is normally short in microgrids.

Fig. 3.1 shows power loss (P_{loss}) characteristic of two different DGs whose parameters are listed in Table 3.1 as DG1 and DG2. Fig. 3.1(b) shows power-loss characteristic under various active power and Fig. 3.1(c) shows power-loss characteristic under various reactive power. Fig. 3.1 shows that power loss of DG varies with variation of either active or reactive power. In addition, different DGs have different power loss behaviours, which provides a possibility to reduce system total power loss by adjusting power distribution among DGs. Taking the example shown in Fig. 3.1(d), DG1 and DG2 should work at points A and B with traditional droop controller, but the system power loss can be reduced by regulating DG1 to A' and DG2 to B'. To describe the idea more clearly, system efficiency curves are plotted under different power distribution ratios with various load conditions in Fig. 3.2. It can be seen that: (1) Conventional power distribution fails to ensure optimum system efficiency under different load profiles; (2) Power distribution ratio that implements optimum system efficiency varies with varying load conditions. It leads to one question what is the mathematical relationship between power distribution and optimum system efficiency.

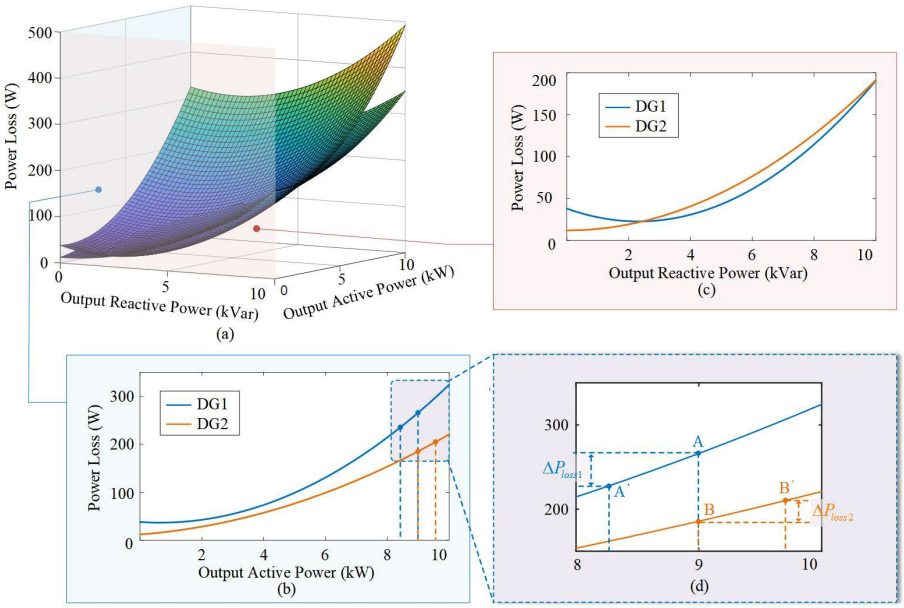

Fig. 3.1. Power loss behaviours of different DGs [69].

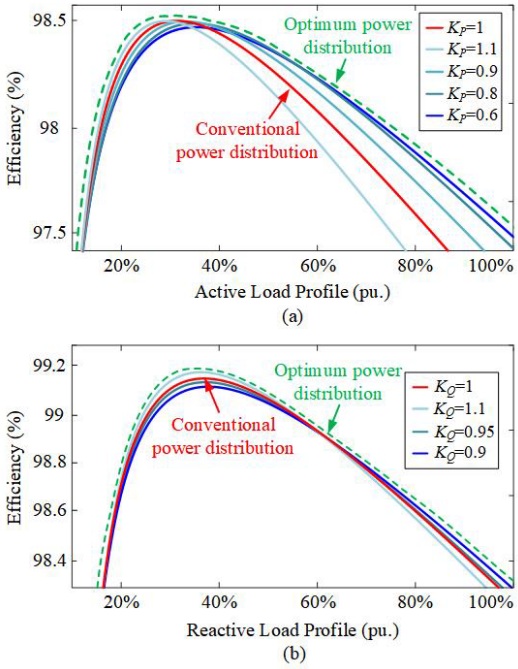

Fig. 3.2. Operation efficiency curves under different power distribution ratios (K_P=P_1/P_2, K_Q=Q_1/Q_2) [69].

3.2.2. SYSTEM EFFICIENCY MODELLING

To make sense the question, optimization model of system efficiency is first built and the optimum conditions are obtained by Lagrange Multiplier Method.

System efficiency of a microgrid is defined as (3-1) [41].

$$\eta_{sys} = \frac{P_{load}}{P_{load} + P_{loss\_tot}} \tag{3-1}$$

where

$$P_{loss\_tot} = \sum_{i=1}^{N} P_{loss\_i} \tag{3-2}$$

$$P_{loss\_i} = a_i P_i^2 + b_i P_i + c_i Q_i^2 + d_i Q_i + e_i P_i Q_i + h_i \tag{3-3}$$

Where P_i and P_{loss_i} is the output power and power loss of DG as shown in Fig. 3.3, N is the number of paralleled DGs in a microgrid, P_{loss_tot} is the total system power loss, a_i, b_i, c_i, d_i, e_i and h_i are coefficients that can be obtained by fitting experimental data.

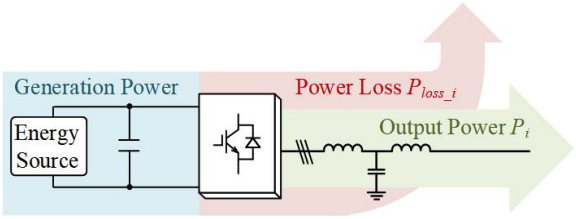

Fig. 3.3. Diagram of power loss and output power of DG.

Then, the system efficiency optimization modelling can be formulated as (3-4) [69].

$$\begin{aligned} &\min\left(P_{loss\_tot}\right) \\ &s.t. \begin{cases} \sum_{i=1}^{N} P_i = P_{load}, \sum_{i=1}^{N} Q_i = Q_{load} \\ f_{\min} \le f_i \le f_{\max}, V_{\min} \le V_i \le V_{\max} \end{cases} \end{aligned} \tag{3-4}$$

To solve the optimization problem, the Lagrange function is introduced as (3-5) [69].

$$L = P_{loss\_tot} + \lambda_1 \left(P_{load} - \sum_{i=1}^{N} P_i \right) + \lambda_2 \left(Q_{load} - \sum_{i=1}^{N} Q_i \right) \tag{3-5}$$

where λ_1 and λ_2 are Lagrange multipliers. Then, the optimum condition can be derived as (3-7) by solving (3-6) [69].

$$\begin{cases} \dfrac{\partial L}{\partial P_1}=0,\ \dfrac{\partial L}{\partial P_2}=0,\ \ldots,\ \dfrac{\partial L}{\partial P_n}=0, \dfrac{\partial L}{\partial Q_1}=0,\ \dfrac{\partial L}{\partial Q_2}=0,\ \ldots,\ \dfrac{\partial L}{\partial Q_n}=0 \\ \dfrac{\partial L}{\partial \lambda_1}=P_{load}-\sum_{i=1}^{N}P_i=0, \dfrac{\partial L}{\partial \lambda_2}=Q_{load}-\sum_{i=1}^{N}Q_i=0 \end{cases} \tag{3-6}$$

$$\begin{cases} \dfrac{\partial P_{loss\_1}}{\partial P_1}=\dfrac{\partial P_{loss\_2}}{\partial P_2}=\cdots=\dfrac{\partial P_{loss\_n}}{\partial P_n},\ \sum_{i=1}^{N}P_i=P_{load} \\ \dfrac{\partial P_{loss\_1}}{\partial Q_1}=\dfrac{\partial P_{loss\_2}}{\partial Q_2}=\cdots=\dfrac{\partial P_{loss\_n}}{\partial Q_n},\ \sum_{i=1}^{N}Q_i=Q_{load} \end{cases} \tag{3-7}$$

Equation (3-7) reveals the core conditions of optimum system efficiency: the system efficiency is optimum when the incremental power losses of all DGs with respect to output active/reactive power are equal.

3.3. EFFICIENCY-PRIORITIZED DROOP CONTROLLER

To improve system efficiency, an efficiency-prioritized droop controller is proposed according to the optimum condition (3-7). Fig. 3.4 shows diagram of the proposed control strategy. Coefficients of power loss are computed by off-line calculation according to (3-3), which are then used in proposed controller to implement optimum active power distribution. Then, an impedance compensation is followed to adjust the equivalent impedance of DG, ensuring optimum reactive power distribution.

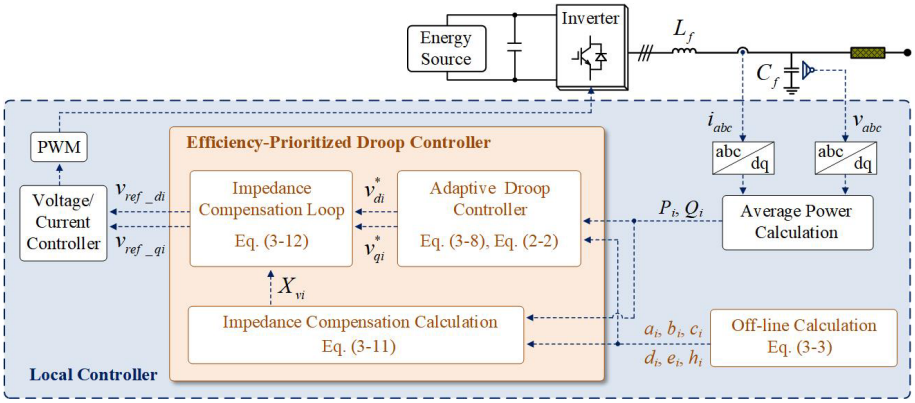

Fig. 3.4. Diagram of the proposed controller [69].

3.3.1. ADAPTIVE DROOP CONTROLLER

To ensure the optimum conditions related to active power in (3-7), the proposed adaptive *P*-ω droop controller is given as (3-8) [69].

$$\begin{cases} \omega_i^* = \omega_{0i}' - m_i' P_i \\ \omega_{0i}' = \omega_0 - k_P \left(b_i + e_i Q_i \right) \\ m_i' = 2 k_P a_i \end{cases} \tag{3-8}$$

where ω_{0i}' and m_i' are retuned droop coefficients according to power loss characteristics of DGs. k_P is a constant that is same for all DGs.

The core of the adaptive *P*-ω droop controller is actually a ($\partial P_{loss}/\partial P$)-$\omega$ droop controller, which can be given as (3-9) by substituting the second and third terms of (3-8) into the first term of (3-8) [69].

$$\omega_i^* = \omega_0 - k_P \frac{\partial P_{loss\_i}}{\partial P_i} \tag{3-9}$$

The principle of proposed controller is shown in Fig. 3.5, taking two same-rating DGs as an example. Fig. 3.5 (a) shows the control curve of traditional droop controller, where the load power is shared equally. Fig. 3.5 (b) shows the control curve of proposed droop controller, where the idea is changing the *x*-axis variable from P_i to $\partial P_{loss\_i}/\partial P_i$. Under the proposed controller, (3-10) can be ensured since $\omega_1 = \omega_2$ in steady state [69], which means that the first term of the optimum conditions is satisfied. Fig. 3.5 (c) shows the equivalent *P*-ω curve under proposed controller, where the active power distribution is adjusted to satisfy the optimum conditions.

$$\frac{\partial P_{loss\_1}}{\partial P_1} = \frac{\partial P_{loss\_2}}{\partial P_2} \tag{3-10}$$

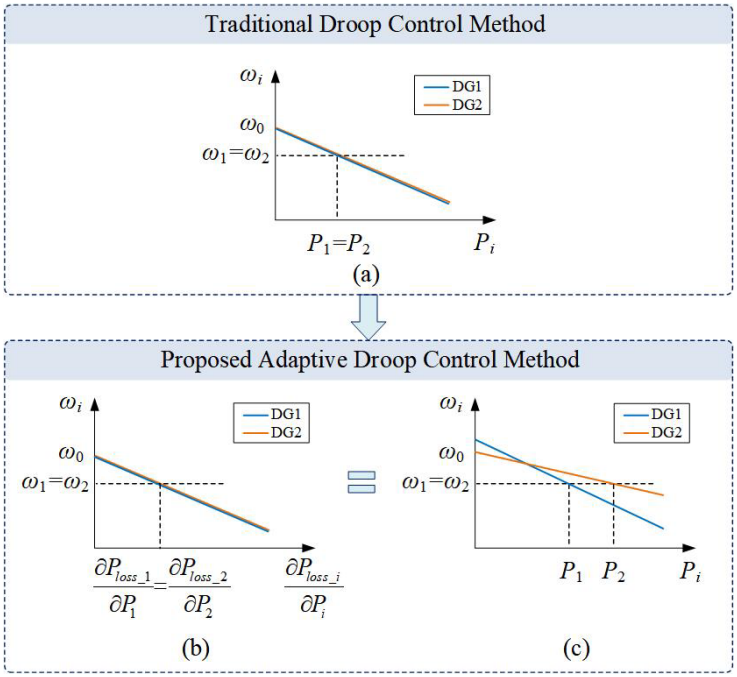

Fig. 3.5. Principle of the proposed droop controller [69]. (a) Traditional P-ω curve. (b) Proposed ($\partial P_{loss}/\partial P$)-$\omega$ curve. (c) Proposed P-ω curve.

3.3.2. IMPEDANCE COMPENSATION LOOP

To perform optimum reactive power sharing for efficiency improvement, a dynamic impedance loop as (3-11) is added to adjust output impedances of DGs based on the second optimum condition in (3-7) [69].

$$\begin{cases} X_{vi}=X_{oi}^{*}-X_{oi} \\ X_{oi}^{*}=\left(2c_i+\dfrac{d_i+e_iP_i}{Q_i}\right)k_Q \end{cases} \tag{3-11}$$

where X_{oi} is output impedance of DG without the impedance compensation loop, whose details can be found in Section 2.2.3. X_{oi}^{*} is the equivalent output impedance after the impedance compensation. k_Q is a constant that is same for all DGs.

Voltage reference after the impedance compensation can be obtained as (3-12) [69].

$$\begin{cases} v_{ref\_di}=v_{di}^{*}+X_{vi}i_{oqi} \\ v_{ref\_qi}=v_{qi}^{*}-X_{vi}i_{odi} \end{cases} \tag{3-12}$$

where v_{di}^* and v_{qi}^* are references from proposed adaptive droop controller, i_{odi} and i_{oqi} are current measurement of DG. v_{ref_di} and v_{ref_qi} are retuned voltage references after the proposed impedance compensation loop.

Under the proposed impedance compensation method, the equivalent output impedance of DG is shown in Fig. 3.6 and reactive-power-distribution ratio is derived as (3-13) [70].

$$\frac{Q_1}{Q_2}=\frac{X_{o2}+X_{v2}}{X_{o1}+X_{v2}}=\frac{X_{o2}^*}{X_{o1}^*}=\frac{2c_2+\dfrac{d_2+e_2P_2}{Q_2}}{2c_1+\dfrac{d_1+e_1P_1}{Q_1}} \tag{3-13}$$

Combining (3-3) and (3-13), (3-14) can be obtained, which means the second optimum condition in (3-7) is ensured by the developed impedance compensation control strategy [69].

$$\frac{\partial P_{loss\_1}}{\partial Q_1}=\frac{\partial P_{loss\_2}}{\partial Q_2} \tag{3-14}$$

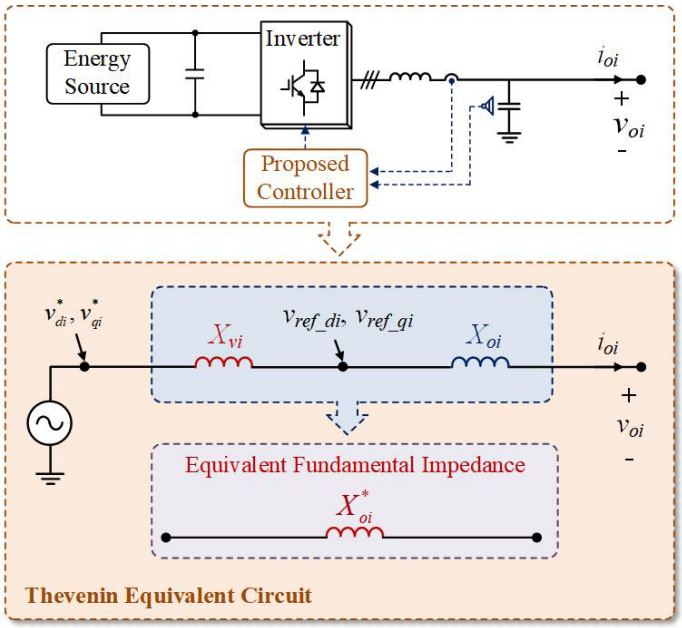

Fig. 3.6. Thevenin equivalent circuit under the proposed impedance compensation method [69].

3.4. SIMULATION AND EXPERIMENTAL VALIDATION

3.4.1. SIMULATION VALIDATION

To validate the performance of proposed control method, a two-DG microgrid is used to execute simulation cases, whose circuit configuration are shown in Fig. 3.7. Simulations are executed in MATLAB/SIMULINK with PLECS blockset. In order to simulate the power loss behaviours, inverter models are built in PLECS with thermal models as shown in Fig. 3.7 according to datasheet [71]-[73]. Simulation parameters are given in Table 3.1. DG1 and DG2 are two same-rating DGs but with different power devices, which are applied to verify the controller under same-rating DGs. DG3 has different power rating with DG1, which is used to verify the controller under DGs with different power ratings by replacing DG2 in Fig. 3.7.

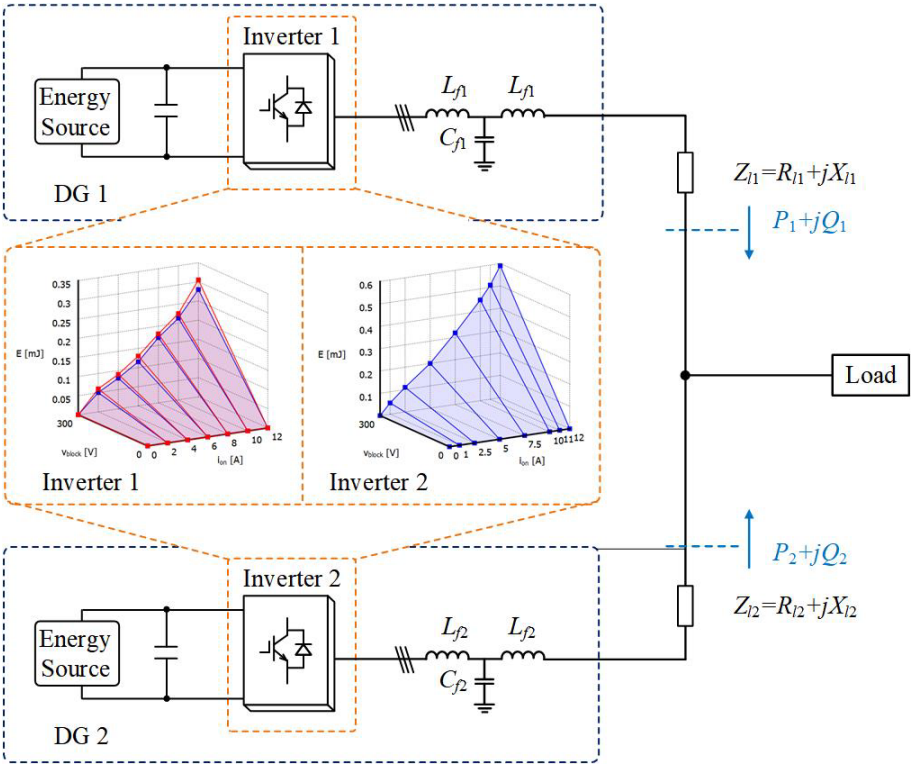

Fig. 3.7. Circuit configuration of the simulation test.

Table 3.1. Simulation Parameters [69]

DG Parameters			
	DG1	DG2	DG3
Manufacturer	Infineon	Semikron	Semikron
Power device	FS6R06VE3_B2	SKiiP 01NEC066V3	SK30GD066ETp
Rated maximum power	P_{Max1}=10kW Q_{Max1}=10kVar	P_{Max2}=10kW Q_{Max2}=10kVar	P_{Max3}=30kW Q_{Max3}=30kVar
DC voltage	V_{dc1}=600V	V_{dc2}=600V	V_{dc3}=600V
Power loss coefficients	a_1=3.29e-6 b_1=-4.28e-3 c_1=2.84e-6 d_1=-1.32e-2 e_1=1.54e-7 h_1=38.14	a_2=1.59e-6 b_2=4.94e-3 c_2=1.79e-6 d_2=1.49e-5 e_2=-5.02e-7 h_2=12.14	a_3=2.33e-7 b_3=5.38e-3 c_3=2.32e-7 d_3=6.42e-3 e_3=-2.13e-7 h_3=28.38
Circuit Parameters			
Filter parameters	$L_{f1}=L_{f2}=L_{f3}$=4mH $C_{f1}=C_{f2}=C_{f3}$=25μF	Line impedance	Z_{l1}=(0.1+j0.63) Ω $Z_{l2}=Z_{l3}$=(0.15+j1.26) Ω
Control Parameters			
Adaptive droop coefficient	k_P=15		
Impedance compensation coefficient	k_Q=2e5		
Switching frequency	$f_{sw1}=f_{sw2}=f_{sw3}$ =10kHz		

Case I: DGs with same power rating

DG1 and DG2 as shown in Table 3.1 are used in this case, where the DGs have same power ratings but different power loss behaviours. To test the effectiveness of the designed controller under various load conditions, load is changed at 0.5s, 1s and 1.5s. Fig. 3.8(a)-(b) show power distribution performance with traditional droop controller and Fig. 3.8(c)-(d) show power sharing behaviour under the designed control method. Under traditional droop controller, load is shared equally even though the power loss behaviours of two DGs are different. With the proposed controller, power distribution ratio is adaptively regulated under various load profiles to improve system efficiency. Fig. 3.8(e) shows system efficiency performances and efficiency improvement under traditional and proposed droop controllers, where efficiency improvement η_{imp} is defined as (3-15). Simulation results show that system efficiency can be enhanced under a different load profiles.

$$\eta_{\text{imp}} = \frac{\eta_{\text{pro}} - \eta_{\text{con}}}{\eta_{\text{con}}} \cdot 100\% \tag{3-15}$$

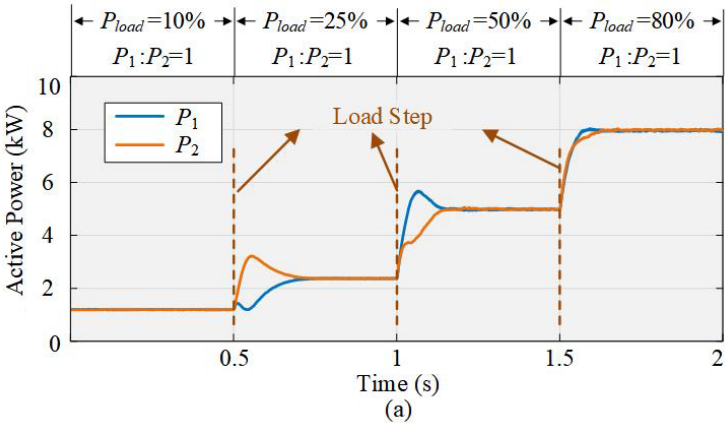

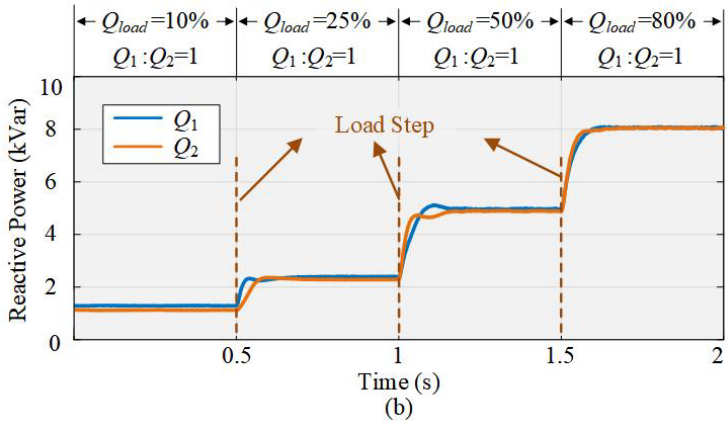

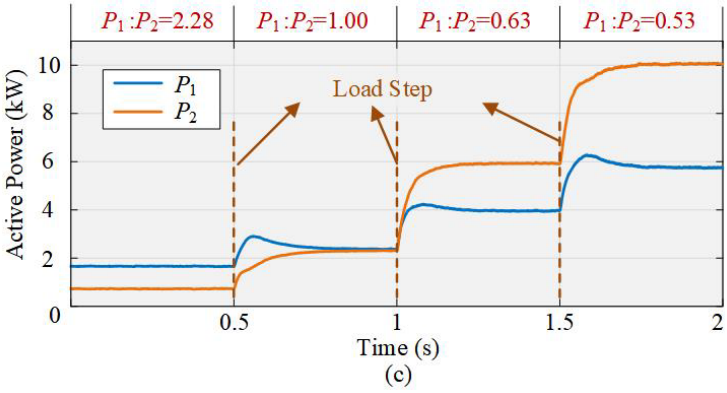

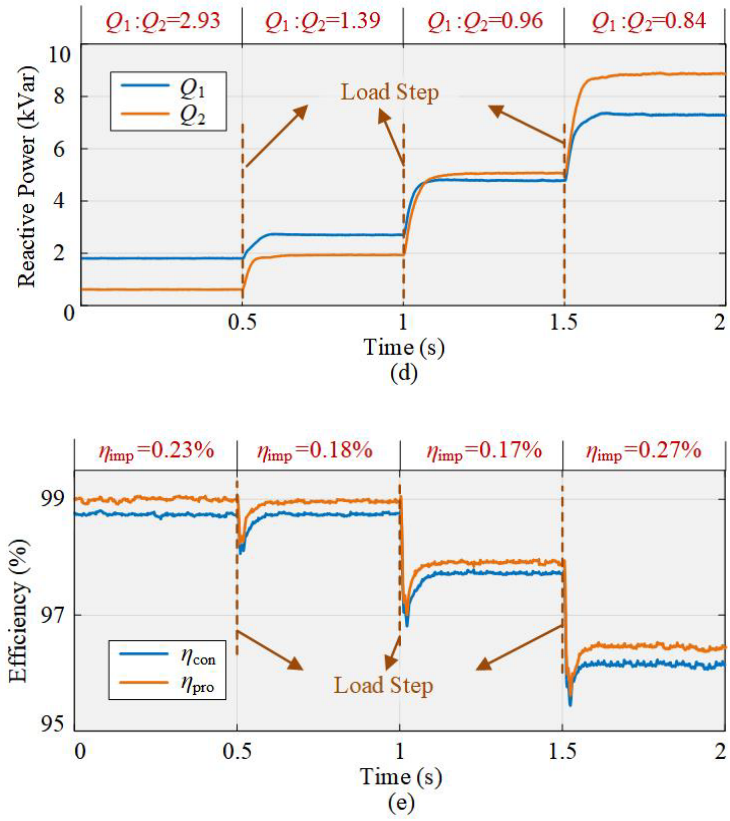

Fig. 3.8. Simulation results of case I [69]. (a) Active-power distribution under traditional droop controller. (b) Reactive-power distribution under traditional droop controller. (c) Active-power distribution under the proposed controller. (d) Reactive-power distribution under the proposed controller. (e) System efficiency under traditional and proposed droop controllers.

Case II: DGs with different power ratings

In this case, by replacing DG2 to DG3 in Table 3.1, DG1 and DG3 are used to validate the proposed controller under DGs with different power capacities. Fig. 3.9(a)-(d) show power distribution under traditional and the proposed droop controllers. Fig. 3.9 (e) shows the system efficiency performance comparison under traditional droop controller and the proposed controller. Simulation results show that for different-rating DGs, the proposed controller is also able to enhance the system efficiency under various load conditions.

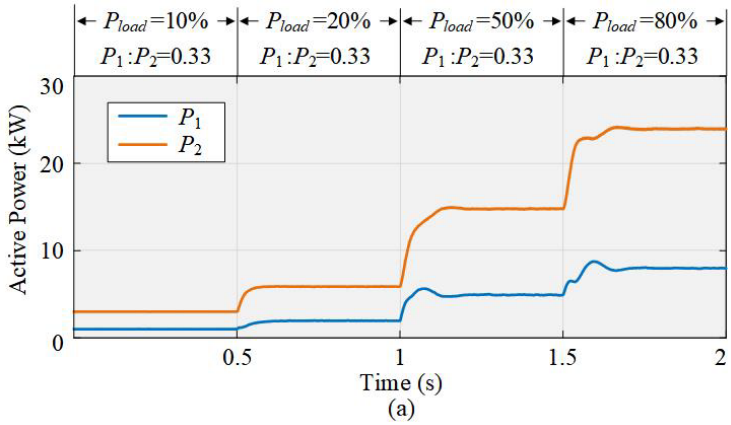
P_{load}=10%
P_{load}=20%
P_{load}=50%
P_{load}=80%
P_1:P_2=0.33
P_1:P_2=0.33
P_1:P_2=0.33
P_1:P_2=0.33
P_1
P_2
Active Power (kW)
Time (s)
(a)

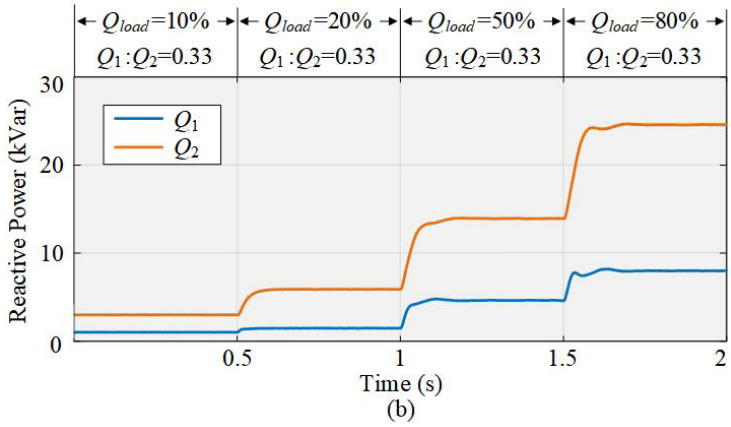
Q_{load}=10%
Q_{load}=20%
Q_{load}=50%
Q_{load}=80%
Q_1:Q_2=0.33
Q_1:Q_2=0.33
Q_1:Q_2=0.33
Q_1:Q_2=0.33
Q_1
Q_2
Reactive Power (kVar)
Time (s)
(b)

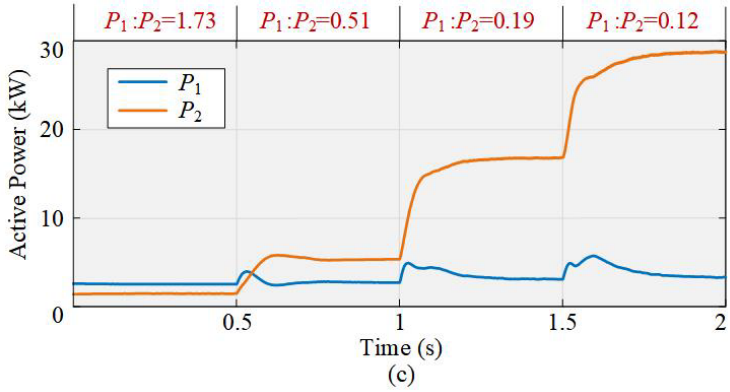
P_1:P_2=1.73
P_1:P_2=0.51
P_1:P_2=0.19
P_1:P_2=0.12
P_1
P_2
Active Power (kW)
Time (s)
(c)

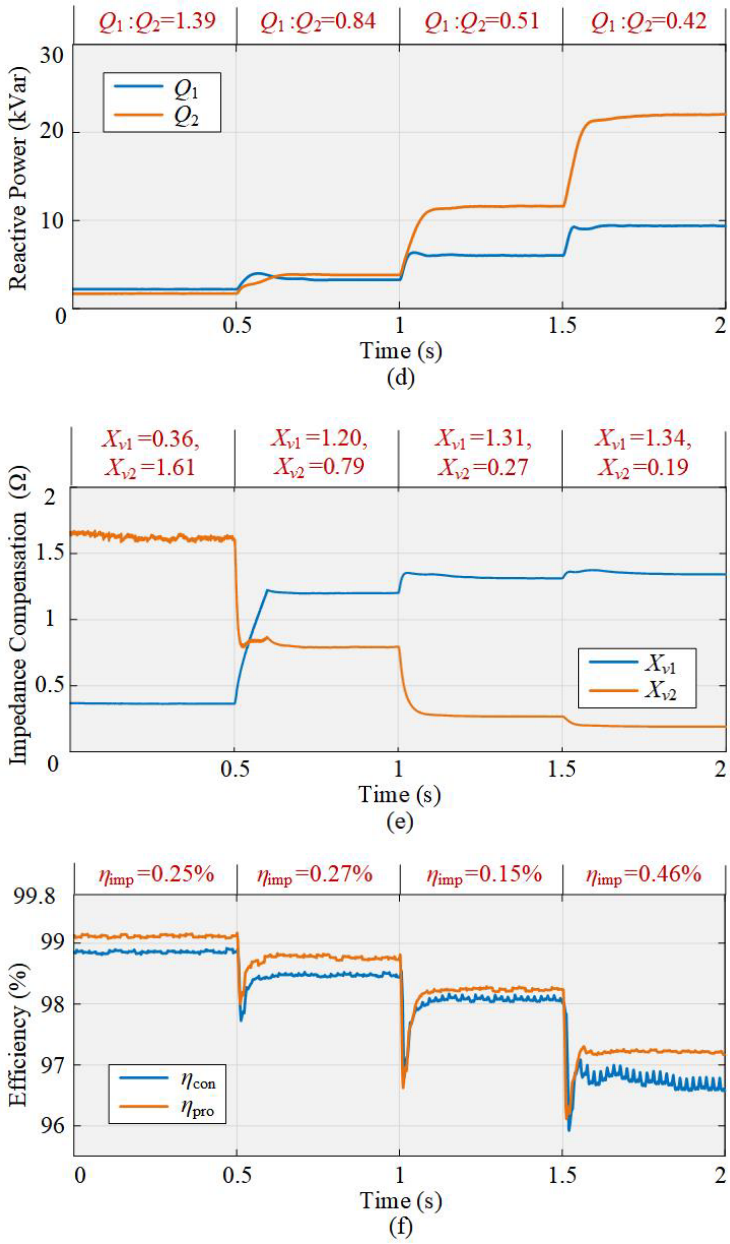

Fig. 3.9. Simulation results of case II [69]. (a) Active-power distribution under traditional droop controller. (b) Reactive-power distribution under traditional droop controller. (c) Active-power distribution under the proposed controller. (d) Reactive-power distribution under the proposed controller. (e) System efficiency under traditional and proposed droop controllers.

3.4.2. EXPERIMENTAL VALIDATION

Experiment is executed to further test the proposed controller, where two same-rating DGs with different power loss characteristics are equipped. The experimental prototype is illustrated in Fig. 3.10, where dSPACE 1006 is equipped to control the system. Power loss data of the DGs are measured under various active power load, as shown in Fig. 3.11. And the power loss coefficients are fitted, which is given in Table 3.2. Fig. 3.12 shows theoretical efficiency curves of the experimental system under traditional controller (blue curve) and the proposed controller (red curve). The theoretical efficiency improvement is also shown in Fig. 3.12 (green curve).

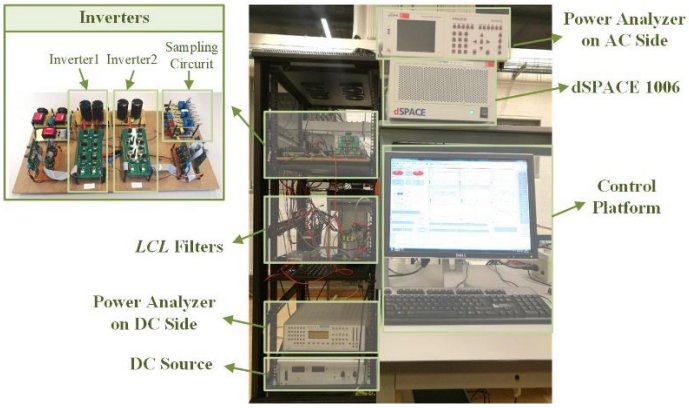

Fig. 3.10. Experimental prototype [69].

Table 3.2. Experimental Parameters [69]

DG Parameters			
		DG1	DG2
Power device	IGBT	IRG4BH20K-SPbF	IXYP30N120C3
	Diode	STTH1512	STTH1512
DC voltage		V_{dc1}=200V	V_{dc2}=200V
Power loss coefficients		a_1=1.75e-5 b_1=8.58e-2 h_1=10.05	a_2=9.58e-5 b_2=4.50e-2 h_2=6.26
Circuit Parameters			
Filter parameters	L_{f1}=1.8mH, C_{f2}=25μF L_{f2}=1.5mH, C_{f2}=25μF	Line impedance	Z_{l1}=(0.01+j0.63) Ω Z_{l2}=(0.02+j1.26) Ω
Control Parameters			
Adaptive droop coefficient		k_P=15	
Impedance compensation coefficient		k_Q=2e5	
Switching frequency		f_{sw1}=f_{sw2} =10kHz	

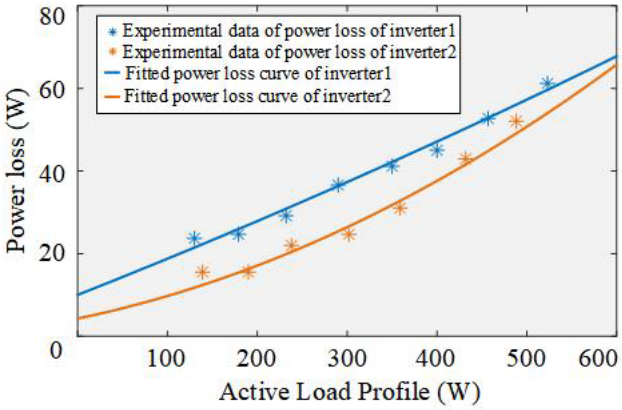

Fig. 3.11. Experimental data and fitted curves of power loss of two DGs [69].

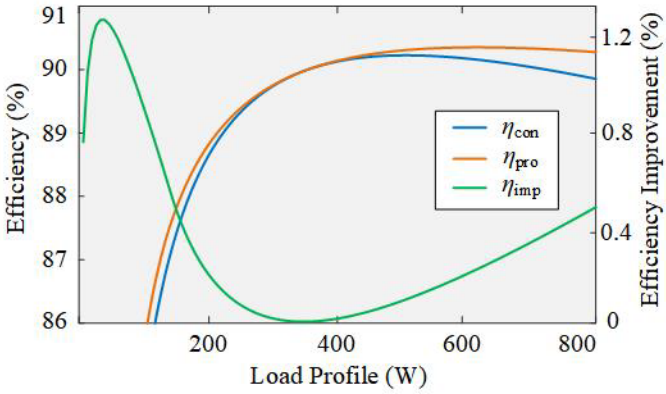

Fig. 3.12. Theoretical system efficiency curves and efficiency improvement curve [69].

Fig. 3.13 shows the A-phase currents of two DGs under the proposed controller. Experimental result shows that the power distribution is adaptively regulated under different load conditions. Table 3.3 shows experimental data about efficiency improvement, which verifies the capability of proposed controller to improve system efficiency. The data also aligns with the theoretical calculation in Fig. 3.12, which indicates the effectiveness of the proposed efficiency optimization model.

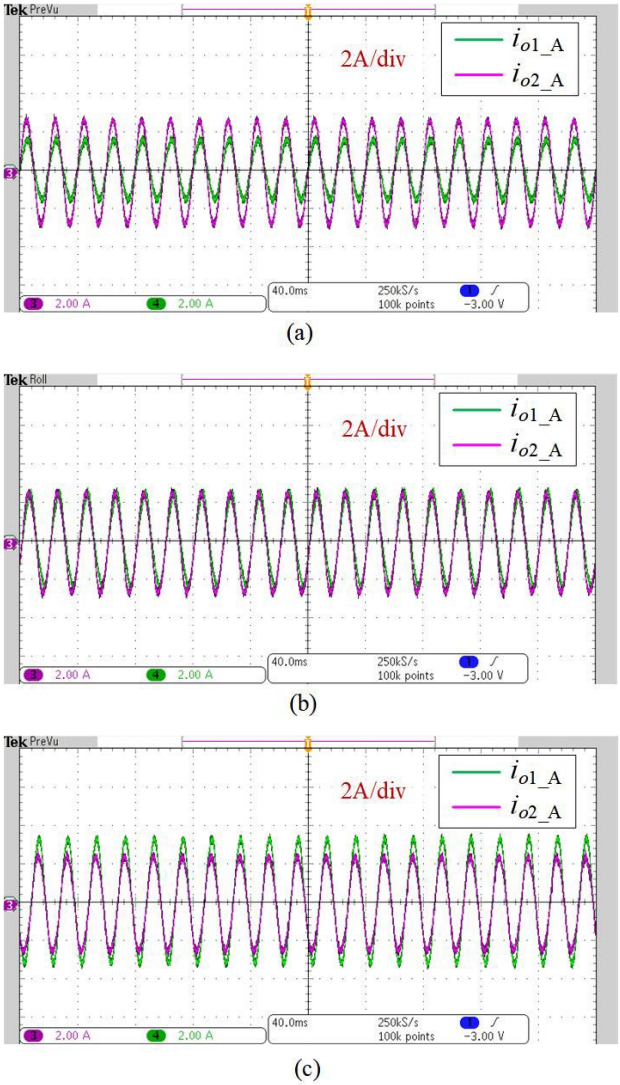

Fig. 3.13. Experimental results with the proposed controller [69]. (a) Phase-A currents of DGs under P_{load}=280W. (b) A-phase currents of DGs under P_{load}=380W. (c) Phase-A currents of DGs under P_{load}=500W.

Table 3.3. Results of Improved Efficiency in Experiment [69]

Load Profiles (W)	280	330	380	430	500
η_{imp} (%)	0.19	0.08	0.02	0.05	0.23

3.5. SUMMARY

This chapter presents an efficiency-prioritized droop controller to improve system efficiency. Efficiency optimization model of microgrids is first built. Optimum conditions of the model are then obtained via Lagrange Multiplier Method. Further, an efficiency-prioritized droop controller is designed to enhance system efficiency. Simulation and experimental results verify the effectiveness of the presented efficiency model and the proposed efficiency-prioritized droop controller.

Chapter 4. Power Sharing Performance of Microgrids Considering System Efficiency and Cost

4.1. ABSTRACT

Apart from system efficiency, operation cost is also an important concern in microgrids. This chapter investigates power distribution performance with consideration of system efficiency and cost at the same time. A multi-objective optimization model is built and optimum conditions are obtained via Lagrange Multiplier Method. A self-optimization droop controller is further designed to improve system performance considering efficiency and cost at the same time.

4.2. MULTI-OBJECTIVE OPTIMIZATION MODELLING CONSIDERING EFFICIENCY AND COST

4.2.1. OPERATION COST MODELLING AND PROBLEM FORMULATION

In renewable-based microgrids, the operation cost of renewable DG is expressed as [61]:

$$C_i = K_{Ci}\left(P_i + P_{loss\_i}\right) \tag{4-1}$$

where K_{Ci} is the cost parameter of DG which is related with emission cost, maintenance cost and storage replacement [54]-[55],[61]. P_i is the output active power of DG. P_{loss_i} is the power loss of DG, which is represented as (3-3) in Section 3.2.2.

Fig. 4.1 shows the power loss and operation cost characteristics of two different DGs (taking DG1 and DG2 in Table 4.1 as an example) with respect to output active power according to (4-1) and (3-3). It can be seen from Fig. 4.1 that there is a tradeoff between operation cost and system efficiency, which thus is difficult to implement the twofold optimization. Therefore, multi-objective optimization method is required to investigate the overall system performance considering system efficiency and operating cost simultaneously.

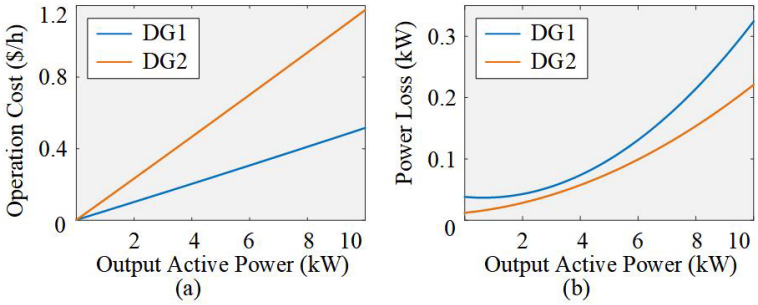

Fig. 4.1. Cost and power loss curves of DGs [74]. (a) Operation cost. (b) Power loss.

4.2.2. MULTI-OBJECTIVE OPTIMIZATION MODELLING

To develop the multi-objective optimization model, a normalized performance factor is defined as (4-2) [74].

$$\begin{aligned} F_i &= \alpha_i \frac{C_i}{C_{\max}} + \beta_i \frac{P_{loss\_i}}{P_{loss\_\max}} \\ &= a_i' P_{oi}^2 + b_i' P_{oi} + c_i' Q_{oi}^2 + d_i' Q_{oi} + e_i' P_{oi} Q_{oi} + h_i' \end{aligned} \tag{4-2}$$

where

$$\begin{cases} 0 \le \alpha_i \le 1,\ 0 \le \beta_i \le 1,\ \alpha_i + \beta_i = 1 \\ C_{\max} = \sum_{i=1}^{N} C_{i\_\max} = \sum_{i=1}^{N} C_i \big|_{P_{oi\_\max}, Q_{oi\_\max}} \\ P_{loss\_\max} = \sum_{i=1}^{N} P_{loss\_i\_\max} = \sum_{i=1}^{N} P_{loss\_i} \big|_{P_{oi\_\max}, Q_{oi\_\max}} \\ a_i' = (\varepsilon_{1i} + \varepsilon_{2i}) a_i,\ b_i' = (\varepsilon_{1i} + \varepsilon_{2i}) b_i + \varepsilon_{1i},\ c_i' = (\varepsilon_{1i} + \varepsilon_{2i}) c_i \\ d_i' = (\varepsilon_{1i} + \varepsilon_{2i}) d_i,\ e_i' = (\varepsilon_{1i} + \varepsilon_{2i}) e_i,\ h_i' = (\varepsilon_{1i} + \varepsilon_{2i}) h_i \\ \varepsilon_{1i} = \dfrac{\alpha_i K_{Ci}}{C_{\max}},\ \varepsilon_{2i} = \dfrac{\beta_i}{P_{loss\_\max}} \end{cases} \tag{4-3}$$

where α_i and β_i are weight coefficients for optimization objectives, which indicates the priorities of cost and efficiency for DG. $C_{\max}$ and $P_{loss\_\max}$ are the maximum cost and power loss of the N-DG microgrid, which is used to normalize the system cost and power loss[75]. a'_i, b'_i, c'_i, d'_i, e'_i and h'_i are normalized performance factors, which are related to weight coefficients, cost coefficient and power loss coefficients of DG.

Then, the multi-objective optimization model is built as (4-4) [74].

$$\min\left(F=\sum_{i=1}^{N}F_i\right)$$
$$s.t.\begin{cases}\sum_{i=1}^{N}P_i=P_{load}\\ \sum_{i=1}^{N}Q_i=Q_{load}\end{cases} \tag{4-4}$$

The Lagrange function is introduced as (4-5) to solve the optimization problem [74].

$$L=F+\gamma_1\left(P_{load}-\sum_{i=1}^{N}P_i\right)+\gamma_2\left(Q_{load}-\sum_{i=1}^{N}Q_i\right) \tag{4-5}$$

where γ_1 and γ_2 are the Lagrange multipliers. The optimum conditions are derived as (4-6) by Lagrange Multiplier Method [74].

$$\begin{cases}\frac{\partial F_1}{\partial P_1}=\frac{\partial F_2}{\partial P_2}=\cdots=\frac{\partial F_n}{\partial P_n},\ \sum_{i=1}^{N}P_i=P_{load}\\ \frac{\partial F_1}{\partial Q_1}=\frac{\partial F_2}{\partial Q_2}=\cdots=\frac{\partial F_n}{\partial Q_n},\ \sum_{i=1}^{N}Q_i=Q_{load}\end{cases} \tag{4-6}$$

To analyze the system performance under different optimization objectives, the comprehensive performance factor F_c is defined as (4-7), and system performance improvement indexes (comprehensive performance reduction F_{c_red}, operation cost saving $C_{\_\mathrm{sav}}$ and system efficiency improvement $\eta_{\_\mathrm{imp}}$) are defined as (4-8) [74].

$$F_c=F\big|_{\alpha_i=0.5,\,\beta_i=0.5} \tag{4-7}$$

$$\begin{cases}F_{c\_\mathrm{red}}=\frac{F_{c\_\mathrm{con}}-F_{c\_\mathrm{pro}}}{F_{c\_\mathrm{con}}}\cdot 100\%\\ C_{\_\mathrm{sav}}=\frac{C_{\_\mathrm{con}}-C_{\_\mathrm{pro}}}{C_{\_\mathrm{con}}}\cdot 100\%\\ \eta_{\_\mathrm{imp}}=\frac{\eta_{\_\mathrm{pro}}-\eta_{\_\mathrm{con}}}{\eta_{\_\mathrm{con}}}\cdot 100\%\end{cases} \tag{4-8}$$

where F_{c_con} , $C_{\_\mathrm{con}}$ and $\eta_{\_\mathrm{con}}$ are system performance factors under traditional power-rating-based power distribution. F_{c_pro}, $C_{\_\mathrm{pro}}$ and $\eta_{\_\mathrm{pro}}$ are factors under the proposed power distribution based on the optimum conditions (4-6). Fig. 4.2 shows system performance factors under different optimization priorities. Case I shows the optimization results under α_i=β_i=0.5, which means the equal priority of operation cost and system efficiency. Case II indicates analysis results under α_i=1 and β_i=0, which

means only operation cost is optimized. Case III shows analysis results under α_i=1 and β_i=0, which refers to single optimization objective for system efficiency. Some connotations can be drawn from Fig. 4.2. (1) The system comprehensive performance can be improved under the whole load profile when operation cost and system efficiency are considered at the same time. (2) F_c can be deteriorated with existing cost-optimized or efficiency-optimized power sharing. When only operation cost is optimized, the system efficiency can be reduced, resulting in a deteriorated F_c, and vice versa. (3) To improve the comprehensive system performance, a tradeoff between system efficiency and operation cost should be made.

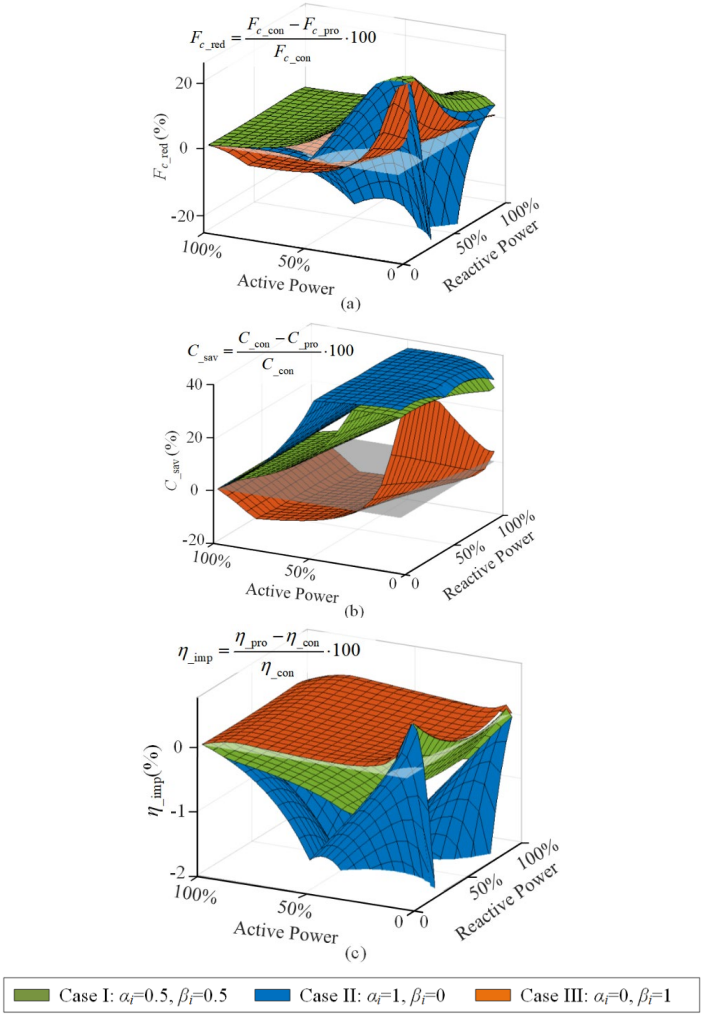

Fig. 4.2. The analysis results of system performance [74]. (a) F_{c_red}. (b) $C_{\_sav}$. (c) $\eta_{\_imp}$.

4.3. POWER CONTROL STRATEGY CONSIDERING EFFICIENCY AND COST

To perform the comprehensive optimization of efficiency and operation cost, a self-optimization droop control method is proposed based on the optimum conditions (4-6), whose diagram is shown in Fig. 4.3. The coefficients of normalized performance factor F_i of each inverter are off-line computed according to (4-2). Then, these coefficients are used in the adaptive droop controller to perform optimum active power distribution. Then a virtual impedance loop is followed to perform the optimum reactive power distribution.

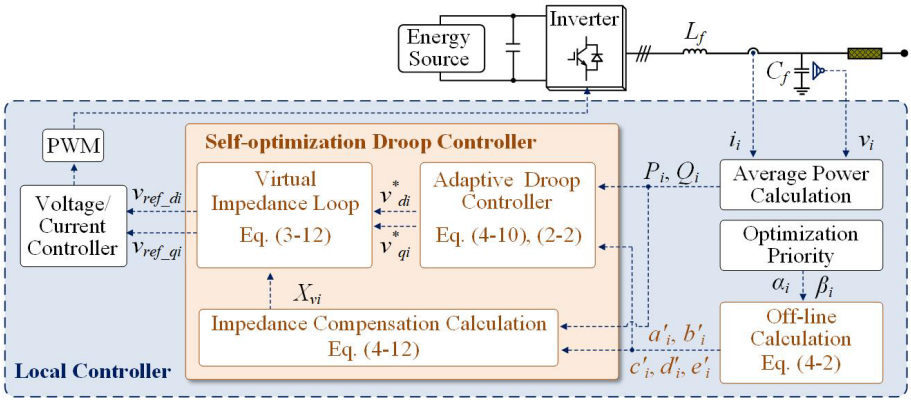

Fig. 4.3. The diagram of the proposed self-optimization droop controller [74].

Similar to the proposed controller in Section 3.3.1, another adaptive active power controller is developed as (4-9), where the *P*-*ω* relationship can be derived as (4-10) [74].

$$\omega_i^* = \omega_0 - k_P \frac{\partial F_i}{\partial P_i} \tag{4-9}$$

$$\begin{cases} \omega_i^* = \omega'_{0i} - m'_i P_i \\ \omega'_{0i} = \omega_0 - k_P \left(b'_i + e'_i Q_i \right) \\ m'_i = 2k_P a'_i \end{cases} \tag{4-10}$$

where ω'_{0i} and m'_i are returned droop coefficients. Different with (3-8), ω'_{0i} and m'_i in (4-10) are adjusted according to parameters of F_i, which is related with power loss coefficients, cost coefficients and weight coefficients together. k_P is an equal constant for all DGs.

Under the adaptive active power control method, (4-11) can be obtained since $\omega_1 = \omega_2$ in steady state, which means the first term of the optimum conditions is satisfied [74].

$$\frac{\partial F_1}{\partial P_1} = \frac{\partial F_2}{\partial P_2} \tag{4-11}$$

To implement the optimum reactive power distribution, a virtual impedance loop as (4-12) is added to change the output impedances of DGs based on the second optimum condition in (4-6) [74].

$$\begin{cases} X_{vi} = X_{oi}^{*} - X_{oi} \\ X_{oi}^{*} = \left(2c_i' + \dfrac{d_i' + e_i' P_i}{Q_i} \right) k_Q \end{cases} \tag{4-12}$$

where X_{oi} is output impedance of DG before the impedance compensation loop. X_{oi}^{*} is the equivalent output impedance after the impedance compensation. k_Q is an equal constant for all DGs.

Under the proposed impedance compensation, the reactive-power-distribution ratio can be derived as (4-13) [70]. Then (4-14) is obtained by combining (4-2) and (4-13), which means the second optimum condition in (4-6) is ensured [74].

$$\frac{Q_{o1}}{Q_{o2}} = \frac{X_{o2} + X_{v2}}{X_{o1} + X_{v2}} = \frac{X_{o2}^{*}}{X_{o1}^{*}} = \frac{2c_2' + \dfrac{d_2' + e_2' P_{o2}}{Q_{o2}}}{2c_1' + \dfrac{d_1' + e_1' P_{o1}}{Q_{o1}}} \tag{4-13}$$

$$2c_1' Q_{o1} + d_1' + e_1' P_{o1} = 2c_2' Q_{o2} + d_2' + e_2' P_{o2} \tag{4-14}$$

4.4. SIMULATION AND EXPERIMENTAL VALIDATION

To validate the performance of proposed self-optimization droop controller, simulation is executed in MATLAB/SIMULINK with PLECS blockset, whose circuit configuration is shown in Fig. 4.4. Simulation parameters are given in Table 4.1 [61],[69].

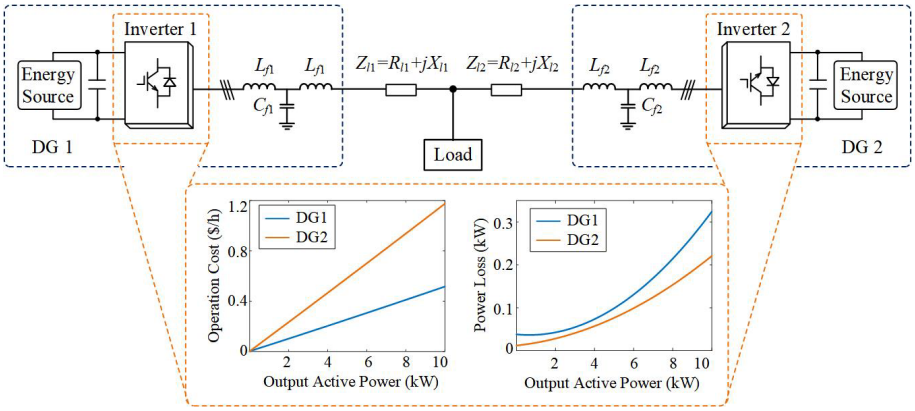

Fig. 4.4. Circuit configuration of the simulation test.

Table 4.1. Simulations Parameters [74]

DG Parameters		
	DG1	DG2
Power device	FS6R06VE3_B2	SKiiP 01NEC066V3
Rated maximum power	P_{Max1}=10kW Q_{Max1}=10kVar	P_{Max2}=10kW Q_{Max2}=10kVar
DC voltage	V_{dc1}=600V	V_{dc2}=600V
Filter parameters	L_{f1}=4mH, C_{f1}=25μF	L_{f1}=2mH, C_{f1}=25μF
Power loss coefficients	a_1=3.29e-6 b_1=-4.28e-3 c_1=2.84e-6 d_1=-1.32e-2 e_1=1.54e-7 h_1=38.14	a_2=1.59e-6 b_2=4.94e-3 c_2=1.79e-6 d_2=1.49e-5 e_2=-5.02e-7 h_2=12.14
Cost coefficients	K_{c1}=0.05	K_{c2}=0.115
Circuit and Control Parameters		
Line impedance	$Z_{l1}=Z_{l2}$=(0.1+j0.63) Ω	
Adaptive droop coefficient	k_P=1.5e3	
Impedance compensation coefficient	k_Q=2e8	
Switching frequency	$f_{sw1}=f_{sw2}=f_{sw3}$ =10kHz	

DG1 and DG2 have same power ratings but different power loss and operation cost behaviours. To test the effectiveness of the proposed controller under various load conditions, load is changed at 0.5s and 1.5s. Fig. 4.5 shows the simulation results under α_i=β_i=0.5, where Fig. 4.5(a)-(b) show power distribution performance with traditional droop controller and Fig. 4.5 (c)-(d) show power distribution under the proposed controller. Under traditional droop controller, load is shared equally even though the power loss and operation cost characteristics of two DGs are different. Under the proposed controller, power-distribution ratio is adaptively regulated under various load profiles to improve system performance. Fig. 4.5 (e)-(g) show system performance behaviours under traditional and proposed controllers. The comprehensive performance is improved by proposed controller. Although system efficiency is slightly reduced, operation cost is saved, which means a tradeoff is made to improve the comprehensive system behaviour.

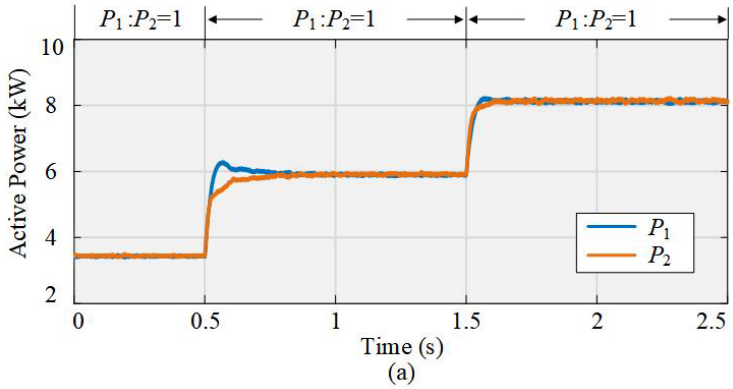

(a)

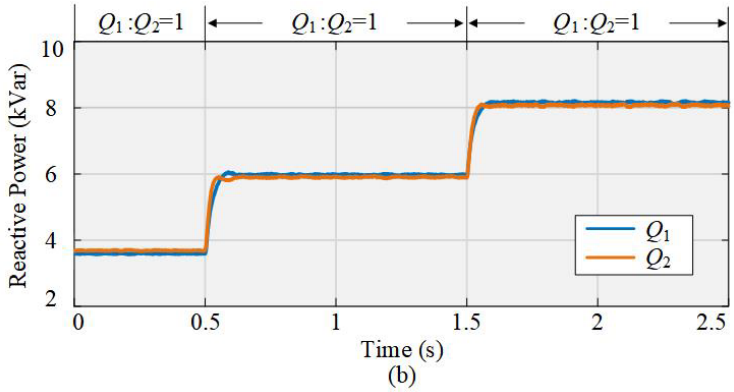

(b)

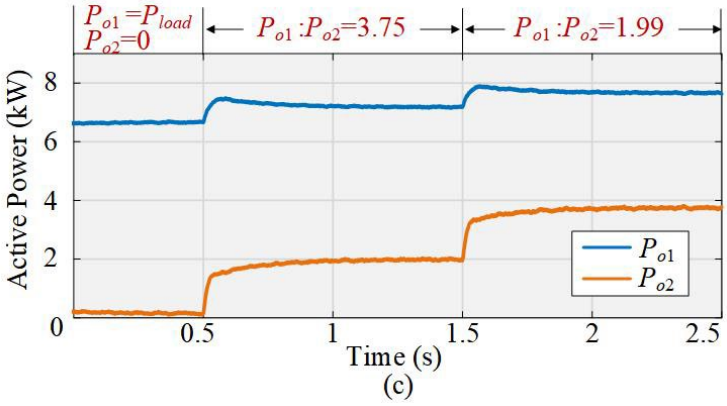
$P_{o1}=P_{load}$
$P_{o2}=0$
$P_{o1}:P_{o2}=3.75$
$P_{o1}:P_{o2}=1.99$
Active Power (kW)
Time (s)
P_{o1}
P_{o2}

(c)

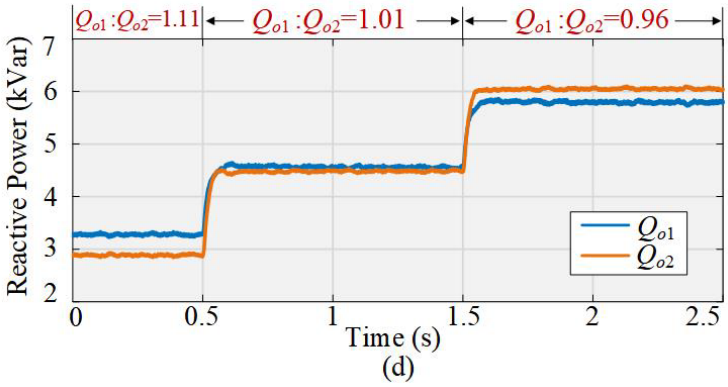
$Q_{o1}:Q_{o2}=1.11$
$Q_{o1}:Q_{o2}=1.01$
$Q_{o1}:Q_{o2}=0.96$
Reactive Power (kVar)
Time (s)
Q_{o1}
Q_{o2}

(d)

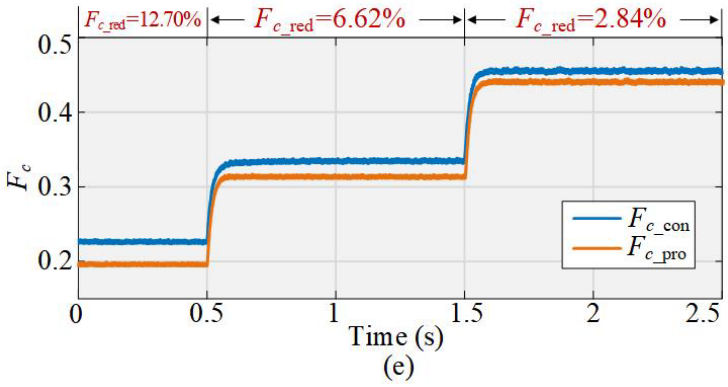
F_{c_red}=12.70%
F_{c_red}=6.62%
F_{c_red}=2.84%
F_c
Time (s)
F_{c_con}
F_{c_pro}

(e)

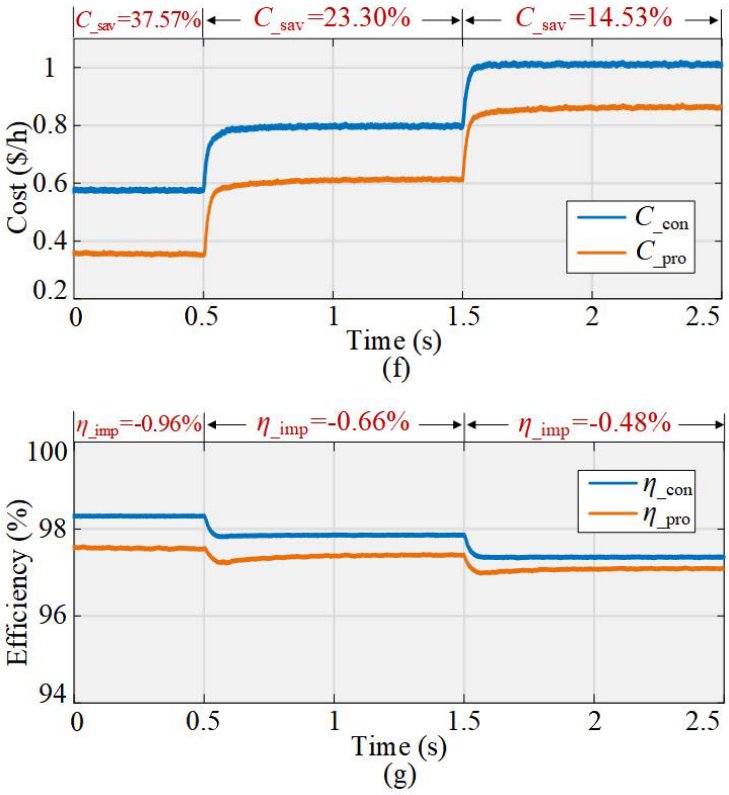

Fig. 4.5. Simulation results [74]. (a) Active-power distribution with traditional droop controller. (b) Reactive-power distribution with traditional droop controller. (c) Active-power distribution with proposed controller. (d) Reactive-power distribution with proposed controller. (e) Comprehensive performance factor with traditional and proposed controller. (f) System efficiency with traditional and proposed controller. (g) Operation cost with traditional and proposed controller.

4.5. SUMMARY

This chapter presents a multi-objective optimization model to analyze system performance, where the model shows that it needs a tradeoff between system efficiency and operation cost to improve system performance. Further, a self-optimization droop controller is proposed to improve comprehensive system behaviour considering operation cost and efficiency at the same time. Simulation results are given to validate the proposed self-optimization droop controller, which shows that the proposed controller is able to improve the overall system performance.

Chapter 5. Conclusions

In this chapter, the outcomes and contributions of the Ph.D. research are summarized and the research perspectives are discussed.

5.1. SUMMARY

The Ph.D. project aims to enhance operation performance of AC microgrids. Several challenges about ensuring desired power control performance, implementing efficiency and cost optimization are addressed by developing decentralized control methods. The summary of this thesis is given as follows.

In Chapter 1, the challenges and motivations of this Ph.D. project is discussed. In AC microgrids, power control performance is a key concern since it is important for system reliability, stability, efficiency and cost. This project aims to improve system power control performance from converter level and system level.

Chapter 2 addresses power sharing control issue for multiple paralleled converters, which aims to analyze and mitigate the impact of nonlinear powder-core filter inductors that is increasingly used in industry. The current-dependent inductor modelling is first built to study the nonlinear characteristic of powder-core filter inductors. The inductor modelling shows that the inductance is actually reduced as load increases because of the inherent soft-saturation characteristic of powder core. System impedance model is then established to investigate the power sharing performance under nonlinear filter inductors, which indicates that the reactive-power-distribution ratio is nonlinear and current-dependent under the impact of nonlinear filter inductors. A robust droop controller is further designed to reduce the impact via nonlinear impedance compensation. Simulation and experimental results show that the nonlinear filter inductors can affect the reactive power distribution behaviour and the proposed controller is able to perform desired power distribution against nonlinear filter inductors.

In system level, one potential challenge is to improve system efficiency by optimizing power control performance, which is discussed in Chapter 3. The efficiency model of microgrid is first built to study the efficiency characteristics under different power distribution ratios. Optimization conditions to ensure the optimum system efficiency are derived by Lagrange Multiplier Method, revealing the core association of power distribution ratios and maximum system efficiency. Furthermore, an efficiency-prioritized droop controller is designed to enhance system efficiency without using communication links. Simulation and experiments are executed to verify the proposed controller, which shows that the designed controller can improve system efficiency under a wide load profile.

In addition to system efficiency, power control performance can also affect system operation cost. Chapter 4 analyzes the relationship between power distribution ratio and system overall performance considering system efficiency and cost together. A multi-objective optimization model is first built to deal with the tradeoff issue between efficiency improvement and cost saving. The optimum conditions of the multi-objective optimization model are obtained via Lagrange Multiplier Method. A self-optimization droop controller is further proposed to improve system comprehensive behaviour considering operation cost and efficiency at the same time. Simulation is also executed to verify the effectiveness of the proposed analysis and control method.

5.2. CONTRIBUTIONS

Main contributions of the Ph.D. project are summarized as follows:

(1) **Desired power control performance against nonlinear components**

- Current-dependent inductor model is established to investigate nonlinear characteristics of powder-core inductors under varying load profiles.
- The influence of nonlinear filter inductors on system power-distribution performance is analyzed by involving nonlinear inductor modelling in system impedance model.
- A robust droop controller is developed to perform desired power sharing performance against the impact of nonlinear filter inductors.

(2) **System efficiency improvement**

- System efficiency model is built to study the system efficiency characteristic under different power-distribution ratios.
- Optimization conditions of the efficiency model are derived to reveal the core association between power distribution ratio and system efficiency.
- A decentralized controller is designed to improve system efficiency.

(3) **System overall performance enhancement**

- A multi-objective optimization model is built to analyze the tradeoff issue between efficiency improvement and cost saving.
- The optimum conditions of the multi-objective optimization model are obtained via Lagrange Multiplier Method.
- A self-optimization droop controller is proposed according to the optimum conditions, improving system comprehensive behaviour.

5.3. RESEARCH PERSPECTIVES

Although several challenges of the power control performance of AC microgrids have been discussed in this Ph.D. project, there are still some potential challenges that should be addressed:

(1) The impact of filter inductor on power-distribution performance is analyzed in this project. Besides, there are other nonlinear factors, such as dead-time effect, can also affect system performance, which needs to be further investigated.

(2) System efficiency model is provided in this project under the datasheet of new devices (IGBTs and diodes). However, the aging of converter can affect the power loss behaviour of system, which can lead to time-varying operation points of system. For a long-term application, the effect of aging on microgrid performance should be considered.

REFERENCES

[1] R. Lasseter, “Smart distribution: Coupled microgrids,” *Proc. IEEE*, vol. 99, no. 6, pp. 1074-1082, Jun. 2011.

[2] P. Lin, C. Jin, J. Xiao, X. Li, D. Shi, Y. Tang, and P. Wang, “A distributed control architecture for global system economic operation in autonomous hybrid AC/DC microgrids,” *IEEE Trans. Smart Grid*, vol. 10, no. 3, pp. 2603-2617, May 2019.

[3] T. L. Vandoorn, J. C. Vasquez, J. De Kooning, J. M. Guerrero, and L. Vandevelde, “Microgrids: Hierarchical Control and an Overview of the Control and Reserve Management Strategies,” in *IEEE Industrial Electronics Magazine*, vol. 7, no. 4, pp. 42-55, Dec. 2013.

[4] J. M. Guerrero, L. G. de Vicuña, J. Matas, M. Castilla, and J. Miret, “Output impedance design for parallel-connected UPS inverters with wireless load-sharing control,” *IEEE Trans. Ind. Electron.*, vol. 52, no. 4, pp. 1126-1135, Aug. 2005.

[5] T. V. Hoang and H.-H. Lee, “An adaptive virtual impedance control scheme to eliminate the reactive-power-sharing errors in an islanding meshed microgrid,” *IEEE J. Emerg. Sel. Topics Power Electron.*, vol. 6, no. 2, pp. 966-976, Jun. 2018.

[6] W. Yao, M. Chen, J. Matas, J. M. Guerrero, and Z.-M. Qian, “Design and analysis of the droop control method for parallel inverters considering the impact of the complex impedance on the power sharing,” *IEEE Trans. Ind. Electron.*, vol. 58, no. 2, pp. 576-588, Feb. 2011.

[7] Y. Wang, X. Wang, Z. Chen, and F. Blaabjerg, “Distributed optimal control of reactive power and voltage in islanded microgrids,” *IEEE Trans. Ind. Applicat.*, vol. 53, no.1, pp. 340-349, Feb. 2017.

[8] A. Tuladhar, H. Jin, T. Unger, and K. Mauch, “Control of parallel inverters in distributed AC power systems with consideration of line impedance effect,” *IEEE Trans. Ind. Appl.*, vol. 36, no. 1, pp. 131-138, Jan./Feb. 2000.

[9] W. Yuan, Y. Wang, D. Liu, F. Deng, and Z. Chen, “Robust droop control of AC microgrid against nonlinear characteristic of inductor,” in *Proc. PEDG*, Jun 3-6, 2019, pp. 642-647.

[10] W. Yuan, Y. Wang, D. Liu, F. Deng, and Z. Chen, “Impacts of inductor nonlinear characteristic in multiconverter microgrids: Modeling, analysis, and mitigation,” *IEEE J. Emerg. Sel. Topics Power Electron.,* vol. 8, no. 4, pp. 3333-3347, Dec. 2020.

[11] J. He, Y. W. Li, J. M. Guerrero, F. Blaabjerg, and J. C. Vasquez, “An islanding microgrid power sharing approach using enhanced virtual impedance control scheme,” *IEEE Trans. Power Electron.*, vol. 28, no. 11, pp. 5272-5282, Nov. 2013.

[12] H. Mahmood, D. Michaelson, and J. Jiang, "Accurate reactive power sharing in an islanded microgrid using adaptive virtual impedances," *IEEE Trans. Power Electron.*, vol. 30, no. 3, pp. 1605-1617, Mar. 2015.

[13] R. An, Z. Liu, and J. Liu, "Successive-approximation-based virtual impedance tuning method for accurate reactive power sharing in islanded microgrids," *IEEE Trans. Power Electron.*, vol. 36, no. 1, pp. 87-102, Jan. 2021.

[14] X. Liang, C. Andalib-Bin-Karim, W. Li, M. Mitolo, and M. N. S. K. Shabbir, "Adaptive virtual impedance-based reactive power sharing in virtual synchronous generator controlled microgrids," *IEEE Trans. Industry Applications*, vol. 57, no. 1, pp. 46-60, Jan-Feb. 2021.

[15] Powder Cores-Product Catalog of Magnetics. "Magnetics powder core catalog."

[16] Ferrite Cores-Product Catalog of Magnetics. "Magnetics ferrite core catalog."

[17] G. R. C. Mouli, J. Schijffelen, P. Bauer, and M. Zeman, "Estimation of ripple and inductance roll off when using powdered iron core inductors," in *Proc. PCIM Europe*, 2016, pp. 1-8.

[18] T. F. Wu, M. Misra, L. C. Lin, and C. W. Hsu, "An improved resonant frequency based systematic LCL filter design method for grid-integrated inverter," *IEEE Trans. Ind. Electron.*, vol. 64, no. 8, pp. 6412-6421, Aug. 2017.

[19] Q. Wei, B. Liu, and S. Duan, "Current ripple analysis and controller design for grid-integrated converters considering the soft-saturation nature of the powder cores," *IEEE Trans. Power Electron.*, vol. 33, no. 10, pp. 8827-8837, Oct. 2018.

[20] T. Wang, C. Chen, T. Liu, Z. Chao, and S. Duan, "Current ripple analysis of three-phase vienna rectifier considering inductance variation of powder-core inductor," *IEEE Trans. Power Electron.*, vol. 35, no. 5, pp. 4568-4578, May. 2020.

[21] H. Zhao, D. Dalal, J. K. Jørgensen, M. M. Bech, X. Wang, and S. Munk-Nielsen, "Behavioral modeling and analysis of ground current in medium-voltage inductors," *IEEE Trans. Power Electron.*, vol. 36, no. 2, pp. 1236-1241, Jul. 2020.

[22] M. A. Swihart, "Inductor cores–material and shape choices," Magnetics, Pittsburgh, PA, USA, 2004. [Online]. Available: htts://www.mag-inc.com

[23] S. Jayalath, D. Ongayo, and M. Hanif, "Modelling powder-core inductors for passive filters in inverters using finite element analysis," *Electronics Letters*, vol. 53, no. 3, pp. 179-181, Feb. 2017.

[24] Y. Liu, H. A. Mantooth, J. C. Balda, and C. Farnell, "Realization of high-current variable AC filter inductors using silicon iron powder core," In *Proc. IEEE APEC*, 2017, pp. 855-860.

[25] Y. Liu, H. A. Mantooth, J. C. Balda, and C. Farnell, "A variable inductor based LCL filter for large-scale microgrid application," *IEEE Trans. Power Electron.*, vol. 33, no. 9, pp. 7338-7348, Sep. 2018.

[26] H. Gurleyen, E. Mese, J. H. Kim, and B. Sarlioglu, “Nonlinear analytical model of an inductance considering saturation and temperature variation,” In *Proc. IEEE ECCE*, 2017, pp. 3150-3154.

[27] T. F. Wu, H. S. Nien, C. L. Shen, and T. M. Chen, “A single-phase inverter system for PV power injection and active power filtering with nonlinear inductor consideration,” *IEEE Trans. Ind. Appl.*, vol. 41, no. 4, pp. 1075-1083, Jul./Aug. 2005.

[28] T. F. Wu, M. Misra, Y. Y. Jhang, Y. H. Huang, and L. C. Lin, “Direct digital control of single-phase grid-integrated inverters with LCL filter based on inductance estimation model,” *IEEE Trans. Power Electron.*, vol. 34, no. 2, pp. 1851-1862, Feb. 2019.

[29] C. R. D. Osório, G. G. Koch, H. Pinheiro, R. C. L. F. Oliveira, and V. F. Montagner, “Robust current control of grid-tied inverters affected by *LCL* filter soft-saturation,” *IEEE Trans. Ind. Electron.*, vol. 67, no. 8, pp. 6550- 6561, Aug. 2020.

[30] C. Fei, Q. Li, and F. C. Lee, “Digital implementation of light-load efficiency improvement for high-frequency LLC converters with simplified optimal trajectory control,” *IEEE J. Emerg. Sel. Topics Power Electron.*, vol. 6, no. 4, pp. 1850-1859, Dec. 2018.

[31] F. Deng, Q. Wang, D. Liu, Y. Wang, M. Cheng, and Z. Chen, “Reference submodule-based capacitor monitoring strategy for modular multilevel converters,” *IEEE Trans. Power Electron.*, vol. 34, no. 5, pp. 4711-4721, May 2019.

[32] Z. Tang, M. Su, Y. Sun, B. Cheng, Y. Yang, F. Blaabjerg, and L. Wang, “Hybrid UP-PWM scheme for HERIC inverter to improve power quality and efficiency,” *IEEE Trans. Power Electron.*, vol. 34, no. 5, pp. 4292-4303, May 2019.

[33] Z. Tang, Y. Yang, M. Su, T. Jiang, F. Blaabjerg, H. Dan, and X. Liang, “Modulation for the AVC-HERIC inverter to compensate for deadtime and minimum pulse width limitation distortions,” *IEEE Trans. Power Electron.*, vol. 35, no. 3, pp. 2571-2584, Mar. 2020.

[34] Y. Qin, Y. Yang, S. Li, Y. Huang, S.-C. Tan and S. Hui, “A high efficiency DC/DC converter for high voltage gain high current applications,” *IEEE J. Emerg. Sel. Topics Power Electron.*, vol. 8, no. 3, pp. 2812-2823, Sep. 2020.

[35] B. Jin and X. Yuan, “Topology, efficiency analysis, and control of a four-level π-type converter,” *IEEE J. Emerg. Sel. Topics Power Electron.*, vol. 7, no.2, pp. 1044-1059, Jun. 2019.

[36] Z. Xin, X. Wang, P. C. Loh, and F. Blaabjerg, “Grid-current-feedback control for LCL-filtered grid converters with enhanced stability,” *IEEE Trans. Power Electron.*, vol. 32, no.4, pp. 3216-3228, Jun. 2016.

[37] D. Thenathayalan, L. Chun-gu, and P. Joung-hu, “High-order resonant converter topology with extremely low-coupling contactless transformers,” *IEEE Trans. Power Electron.*, vol. 31, no. 3, pp. 2347-2361, Mar. 2016.

[38] H. Wang, A. M. Khambadkone, and X. Yu. "Control of parallel connected power converters for low voltage microgrid-Part II: Dynamic electro-thermal modeling." *IEEE Trans. Power Electron.,* vol. 25, no. 12, pp. 2971-2980, Dec. 2010.

[39] X. Yu, A. M. Khambadkone, H. Wang, and S. T. S. Terence. "Control of parallel connected power converters for low voltage microgrid-Part I: A hybrid control architecture." *IEEE Trans. Power Electron.,* vol. 25, no. 12, pp. 2962-2970, Dec. 2010.

[40] P. Bartal and I. Nagy, "Game theoretic approach for achieving optimum overall efficiency in DC/DC converters," *IEEE Trans. Ind. Electron.*, vol. 61, no. 7, pp. 3202-3209, Jul. 2014.

[41] S. Wang, J. Liu, Z. Liu, T. Wu, and B. Liu. "Efficiency-based optimization of steady-state operating points for parallel source converters in stand-alone power system." In *Proc. 8th ECCE Asia*, May. 22-26, 2016, pp. 163-170.

[42] L. Meng, T. Dragicevic, J. C. Vasquez, and J. M. Guerrero, "Tertiary and secondary control levels for efficiency optimization and system damping in droop controlled DC-DC converters," *IEEE Trans. Smart Grid.*, vol. 6, no.6, pp. 2615-2626, Jun. 2015.

[43] J.-H. Teng, S.-H. Liao, W.-H. Huang, and C.-C. Chiang, "Smart control strategy for conversion efficiency enhancement of parallel inverters at light loads," *IEEE Trans. Ind. Electron.*, vol. 63, no. 12, pp. 7586–7596, Dec. 2016.

[44] X. Hou, Y. Sun, X. Zhang, J. Lu, P. Wang, and J. M. Guerrero, "Improvement of frequency regulation in VSG-based AC microgrid via adaptive virtual inertia," *IEEE Trans. Power Electron.,* vol.35, no.2, pp.1589-1602, Feb. 2020.

[45] W. Yuan, Y. Wang, X. Ge, X. Hou, and H. Han, "A unified distributed control strategy for hybrid cascaded-parallel microgrid," *IEEE Trans. Energy Convers.*, vol. 34, no. 4, pp. 2029-2040, Dec. 2019.

[46] X. Hou, Y. Sun, H. Han, Z. Liu, W. Yuan, M. Su, "A fully decentralized control of grid-integrated cascaded inverters," *IEEE Trans. Sustainable Energy*, vol. 10, pp.315-317, Jan. 2019.

[47] Y. Wang, Z. Chen, X. Wang, Y. Tian, Y. Tan, and C. Yang, "An estimator-based distributed voltage predictive control strategy for AC islanded microgrids," *IEEE Trans. Power Electron.*, vol. 30, no. 7, pp. 3934-3951, July. 2015.

[48] L. Meng, T. Dragicevic, J. M. Guerrero, and J. C. Vasquez, "Dynamic consensus algorithm based distributed global efficiency optimization of a droop controlled DC microgrid," in *Proc. IEEE Int. Energy Conf. (ENERGYCON)*, May 2014, pp. 1276-1283.

[49] J. Gao, J. Chen, B. Qi, Y. Zhao, K. Peng, and X. Zhang, "A cost-effective two-stage optimization model for microgrid planning and scheduling with compressed air energy storage and preventive maintenance," in *International Journal of Electrical Power & Energy Systems*, vol. 125, pp. 1-14, Feb. 2021.

[50] H. Dunham, D. Cutler, S. Mishra, and X. Li, "Cost-optimal evaluation of centralized and distributed microgrid topologies considering voltage constraints," in *Energy for Sustainable Development*, vol. 56, pp. 88-97, June. 2020.

[51] S. Puradbhat, S. Doolla, and V. Bhavaraju, "A framework for considering capital cost limit in sizing microgrid distributed energy resources-application to industrial microgrids," in *IEEE Transactions on Industry Applications*, vol. 57, no. 6, pp. 6688-6699, Nov.-Dec. 2021.

[52] C. Chen, S. Duan, T. Cai, B. Liu, and G. Hu, "Smart energy management system for optimal microgrid economic operation," *IET Renew. Power Gener.*, vol. 5, no. 3, pp. 258–267, May 2011.

[53] Q. Jiang, M. Xue, and G. Geng, "Energy management of microgrid in grid-integrated and stand-alone modes," *IEEE Trans. Power Syst.*, vol. 28, no. 3, pp. 3380-3389, Aug. 2013.

[54] I. U. Nutkani, P. C. Loh, P. Wang, and F. Blaabjerg, "Autonomous droop scheme with reduced generation cost," *IEEE Trans. Ind. Electron.*, vol. 61, no. 12, pp. 6803–6811, Dec. 2014.

[55] I. U. Nutkani, P. C. Loh, and F. Blaabjerg, "Droop scheme with consideration of operating costs," *IEEE Trans. Power Electron.*, vol. 29, no. 3, pp. 1047–1052, Mar. 2014.

[56] A. Elrayyah, F. Cingoz and Y. Sozer, "Construction of nonlinear droop relations to optimize islanded microgrid operation," in *IEEE Transactions on Industry Applications*, vol. 51, no. 4, pp. 3404-3413, July-Aug. 2015.

[57] F. Chen, M. Chen, Q. Li, K. Meng, Y. Zheng, and J. M. Guerrero, "Costbased droop schemes for economic dispatch in islanded microgrids," *IEEE Trans. Smart Grid*, vol. 8, no. 1, pp. 63-74, Jan. 2017.

[58] J. Reynolds, M. W. Ahmad, Y. Rezgui, and J. Hippolyte, "Operational supply and demand optimisation of a multi-vector district energy system using artificial neural networks and a genetic algorithm," *Applied Energy*, vol. 235, pp. 699-713, Feb. 2019.

[59] M. F. Roslan, M. A. Hannan, Pin Jern Ker, R. A. Begum, T. M. Indra Mahlia, and Z. Y. Dong, "Scheduling controller for microgrids energy management system using optimization algorithm in achieving cost saving and emission reduction," *Applied Energy*, vol. 292, pp. 1-16, June 2021.

[60] Jangkyum Kim, Hyeontaek Oh, and Jun Kyun Choi, "Learning based cost optimal energy management model for campus microgrid systems," *Applied Energy*, vol. 311, pp. 1-15, Jan. 2022.

[61] I. U. Nutkani, P. C. Loh, P. Wang, and F. Blaabjerg, "Decentralized economic dispatch scheme with online power reserve for microgrids," *IEEE Trans. Smart Grid*, vol. 8, no. 1, pp. 139-148, Jan. 2017.

[62] Y. Han, H. Li, P. Shen, E. A. A. Coelho, and J. M. Guerrero, "Review of Active and Reactive Power Sharing Strategies in Hierarchical Controlled Microgrids," *IEEE Trans. Power Electron.*, vol. 32, no. 3, pp. 2427-2451, Mar. 2017.

[63] M. C, Chandorkar, D. M. Divan, and R. Adapa, "Control of parallel connected inverters in standalone ac supply systems," *IEEE Trans. Ind. Appl.,* vol.29, no.1, pp.136-143, Jan.1993.

[64] D. Halliday, R. Resnick, and J. Walker, *Fundamentals of Physics, Chapters 28-31*, 10th ed. John Wiley & Sons, 2010.

[65] A. Isidori, *Nonlinear Control Systems*. New York: Springer-Verlag, 1995.

[66] J. M. Guerrero, L. G. Vicuña, J. Matas, M. Castilla, and J. Miret, "Output impedance design of parallel-connected UPS inverters with wireless load-sharing control," *IEEE Trans. Ind. Electron.*, vol. 52, no. 4, pp. 1126-1135, Aug. 2005.

[67] "Magnetics powder core catalog", 00K6527E026, *Magnetics datasheet*, 2014.

[68] "Magnetics powder core catalog", 00K160LE026, *Magnetics datasheet*, 2013.

[69] W. Yuan, Y. Wang, D. Liu, F. Deng, and Z. Chen, "Efficiency-prioritized droop control strategy of AC microgrid," *IEEE J. Emerg. Sel. Topics Power Electron.,* vol. 9, no. 3, pp. 2936-2950, June 2021.

[70] Y. Wang, D. Liu, P. Liu, F. Deng, D. Zhou, and Z. Chen, "Lifetime-oriented droop control strategy for AC islanded microgrids," *IEEE Trans. Ind. Appl*., vol. 55, no. 3, pp. 3252-3263, Feb. 2019.

[71] "IGBT modules technical information," FS6R06VE3_B2, *Infineon datasheet*, 2013.

[72] "IGBT modules technical information," SKiiP 01NEC066V3, *Semikron datasheet*, 2009.

[73] "IGBT modules technical information," SK30GD066ETp, *Semikron datasheet*, 2015.

[74] W. Yuan, Y. Wang, and Z. Chen, "New perspectives on power control of AC microgrid considering operation cost and efficiency," *IEEE Trans. Power Systems,* vol. 36, no. 5, pp. 4844-4847, Sept. 2021.

[75] N. Srinivas and K. Deb, "Multilingual optimization using nondominated sorting in genetic algorithms," *Evolutionary Computation,* vol.2, no.3 pp.221-248, 1994.

ISSN (online): 2446-1636
ISBN (online): 978-87-7573-785-7

AALBORG UNIVERSITY PRESS